https://doi.org/10.5194/egusphere-2026-6317
Preprint. Discussion started: 11 November 2026
© Author(s) 2026. CC BY 4.0 License.

Climate-Driven Temperature Changes in the Future Impair China's Terrestrial Carbon Sink Capacity

Bowen Xu[1], Jiani Tan[1,2*], Yujian Wang[1], Jinglei Wu[3], Haixia Dai[2], Ling Huang[1], Li Li[1*]

[1]Key Laboratory of Organic Compound Pollution Control Engineering, School of Environmental and Chemical Engineering, Shanghai University, Shanghai 200444, China
[2]Key Laboratory of Formation and Prevention of Urban Air Pollution Complex, Ministry of Ecology and Environment, Shanghai Academy of Environmental Sciences, Shanghai, 200233, China
[3]School of Computer Engineering and Science, Shanghai University, 200444, China

Correspondence to: Jiani Tan (jiani-tan@shu.edu.cn) and Li Li (Lily@shu.edu.cn)

Abstract. The terrestrial carbon sink modulates the rise of atmospheric CO_2, yet its long-term persistence under climate warming remains poorly constrained, largely due to nonlinear temperature responses of ecosystem carbon fluxes. Here we integrate eddy-covariance observations, process-based simulations, and interpretable machine learning to quantify the nonlinear temperature dependence of China's net ecosystem productivity (NEP) and project changes in terrestrial carbon sinks to 2060 across shared socioeconomic pathways. Site-scale observations reveal vegetation-specific turning points in NEP–temperature relationships, yielding a broad range of NEP temperature thresholds spanning 15–25 °C. Aggregated to the national scale, NEP remains stable between 0 and 18 °C, peaks near 20 °C (18–22°C), and declines beyond this optimum threshold, implying that sustained warming could weaken terrestrial carbon sequestration. A controlled sensitivity experiment with uniform 0.5 °C warming reduces national NEP by 0.17 PgC yr^{-1}, corresponding to a 31% loss of the terrestrial carbon sink. Extending this framework to 2060, our projections show national NEP reductions of 24%, 27%, and 56% under SSP1-2.6, SSP2-4.5, and SSP5-8.5, respectively. Across all three scenarios, grasslands exhibit the highest proportional vulnerability to warming, with NEP losses ranging from 44% to 171%, whereas forests show comparatively modest relative NEP declines (7–23%). While land-use and vegetation dynamics can partially offset these sink losses, such buffering effects remain localized and are overwhelmed by nationwide warming-driven carbon sink reduction. Our findings demonstrate that this warming-triggered NEP decline diminishes the capacity of terrestrial ecosystems to buffer atmospheric CO_2 accumulation and mitigate climate change. This study illustrates how threshold-line nonlinear NEP-temperature responses weaken terrestrial carbon sink contributions toward China's carbon peaking and carbon neutrality goals.

https://doi.org/10.5194/egusphere-2026-6317
Preprint. Discussion started: 11 November 2026
© Author(s) 2026. CC BY 4.0 License.

1 Introduction

Terrestrial ecosystems are a major component of the global carbon cycle and provide an important natural buffer against anthropogenic CO_2 emissions (Fu et al., 2022; Ruehr et al., 2023). Their carbon sequestration capacity directly modulates atmospheric CO_2 trajectories under climate change. The global terrestrial carbon sink is approximately 2.0–3.4 Pg C yr^{-1}, with China contributing 13–18% of the total global sink capacity (Jiang et al., 2016; Zhong et al., 2023; Friedlingstein et al., 2022). In recent decades, large-scale afforestation, ecological restoration and vegetation recovery have strengthened China's terrestrial carbon stock, enabling terrestrial ecosystems to offset 21–45% of national fossil-fuel CO_2 emissions (Bai et al., 2024; Xia et al., 2024; Yue et al., 2024). As a result, terrestrial carbon sinks have been regarded as a core long-term offset for China's carbon peaking and carbon neutrality goals. However, the stability of this key carbon sink under continuous future climate warming remains highly uncertain. Rising temperatures may exceed the physiological tolerance thresholds of terrestrial vegetation, potentially constraining carbon sequestration capacity and undermining the sustainability of China's terrestrial carbon sink.

Climate warming shapes terrestrial carbon exchange by regulating vegetation photosynthesis and ecosystem respiration, driving pronounced nonlinear responses of net ecosystem productivity (NEP) to temperature. Moderate warming alleviates cold limitation on vegetation growth, prolongs the growing season, and promotes photosynthetic carbon uptake, thereby enhancing terrestrial carbon sequestration (Piao et al., 2019; Toïgo et al., 2020; Yuan et al., 2025; Friedlingstein et al., 2026). In contrast, excessive warming suppresses photosynthetic efficiency, accelerates respiratory carbon loss, and ultimately reduces net carbon sequestration (Fernández-Martínez et al., 2019; Yuan et al., 2025; Yvon-Durocher et al., 2012; Piao et al., 2019; Toïgo et al., 2020). Collectively, terrestrial carbon fluxes often exhibit a characteristic pattern with NEP increases within a favorable temperature window but may decline sharply beyond a certain statistical turning point (Xu et al., 2025). This threshold-like behavior divides carbon dynamics into cold-limited, favorable-temperature, and heat-stressed regimes, highlighting the necessity of resolving NEP-temperature nonlinear responses for accurate carbon sink projection. Importantly, such statistically-derived turning points represent emergent ecosystem responses shaped by prevailing contemporary environmental conditions.

Such non-linear NEP-temperature responses bring unprecedented uncertainties to regional carbon sink assessment, and this issue is particularly prominent across China due to extreme spatial heterogeneity in climate conditions, terrain features, and vegetation distribution. China covers multiple thermal zones from cold temperate to tropical regions, supporting diverse vegetation types including evergreen forests, deciduous forests, mixed forests, shrublands, croplands, grasslands and savannas. These ecosystems possess divergent functional traits, thermal adaptation strategies and carbon allocation patterns, resulting in large differences in the temperature sensitivity of gross ecosystem exchange (GEE) and ecosystem respiration (ER) (Cramer et al., 2001; Yue et al., 2020). Specifically, high-latitude and high-altitude ecosystems may still benefit from moderate warming via reduced cold limitation, whereas mid- and low-latitude ecosystems are highly vulnerable to excess warming, with temperature overshooting physiological tolerance ranges likely to trigger severe carbon sink degradation. To

https://doi.org/10.5194/egusphere-2026-6317
Preprint. Discussion started: 11 November 2026
© Author(s) 2026. CC BY 4.0 License.

date, a systematic quantification of vegetation-divergent NEP-temperature nonlinear responses across China remains lacking, including the occurrence of statistical turning points within these response curves. Furthermore, the national-scale consequences of shifting along these nonlinear response trajectories for terrestrial carbon-sink stability have not been explicitly clarified. Resolving this knowledge gap is essential to distinguish resilient and vulnerable regions of China's terrestrial carbon sink under future warming.

Current national-scale evaluations of terrestrial carbon-sink capacity are further hindered by inherent methodological limitations in characterizing temperature-driven carbon dynamics and these nonlinear NEP-temperature relationships. Eddy covariance observations provide accurate site-scale carbon flux measurements but suffer from limited spatial representativeness, failing to support national-scale analysis of NEP-temperature responses and future carbon sink projection (Piao et al., 2022). Process-based models can mechanistically simulate photosynthetic and respiratory processes, but their performance is constrained by structural biases, empirical parameterization errors, and large uncertainties in vegetation responses to warming (Amthor et al., 2001; Sitch et al., 2015). Although machine learning techniques can capture complex nonlinear ecological relationships, most existing models lack ecological interpretability for flux-temperature behaviors. None of the conventional methods can effectively integrate multi-source data to systematically quantify these temperature-response patterns and their implications for future carbon sink trajectories, highlighting an urgent need for an integrated analytical framework.

Here, we develop a comprehensive framework integrating field eddy-covariance observations, process-based biogeochemical simulations, and interpretable machine learning to systematically quantify temperature-driven responses of China's terrestrial carbon sink and address the above knowledge gaps. First, we characterize NEP–temperature relationships across seven dominant vegetation types and identify the temperature thresholds where net carbon sequestration transitions from rising to declining. Then, we conduct controlled warming sensitivity experiments to isolate and quantify how uniform temperature elevation alters national NEP. Third, we project spatiotemporal variations in China's terrestrial NEP from 2020 to 2060 under three shared socioeconomic pathways (SSP1-2.6, SSP2-4.5, and SSP5-8.5). We quantify future trajectories of national carbon sink capacity and carbon offset potential under progressive warming, and disentangle how land-use change and vegetation dynamics modulate warming-induced carbon sink weakening. By explicitly linking nonlinear NEP–temperature threshold behaviours to long-term terrestrial carbon sink trajectories, this study reveals how climate warming may degrade China's terrestrial carbon sequestration function, with large contrasts in thermal vulnerability among vegetation functional types. The findings provide targeted scientific support for terrestrial carbon sink management and climate mitigation policymaking in China under future global warming.

https://doi.org/10.5194/egusphere-2026-6317
Preprint. Discussion started: 11 November 2026
© Author(s) 2026. CC BY 4.0 License.

2 Methods

2.1 In-situ measurements of NEP and environmental factors

This study utilized in-situ NEP measurements from ChinaFLUX network to characterize the nonlinear responses of carbon exchange to key climatic factors at the site scale. This dataset provides ground truth for subsequent model calibration and algorithm validation. The carbon fluxes were observed by an eddy covariance system, which utilized sonic anemometers and infrared CO_2/H_2O gas analyzers at 10 Hz frequency. Raw data are reported at 30-min temporal resolution and further subjected to rigorous flux corrections and gap-filling (García-Martínez and Hartshorn, 2023; Yu et al., 2014; Yu et al., 2006; Yu et al., 2008). We collected observations from 21 sites spanning the time period of 2005–2020. The data covered seven major terrestrial ecosystem types (Fig. 1 and Table S1). Key variables used include carbon fluxes (NEP, GEE, and RES) and near-surface air temperature.

Due to the sparse spatial distribution of observational sites, the temperature coverage in the measurement records is limited. For example, only two sites with Deciduous Forest type vegetation are available, all located in North China, with temperatures under 20°C. In contrast, this vegetation type is widely distributed across China, where summer air temperatures can commonly exceed 30 °C in southern China. To examine the relationship between temperature and NEP across China's representative temperature gradients, we separately applied quadratic regression models to fit the relationships between temperature and RES, as well as temperature and GEE (Table S2).

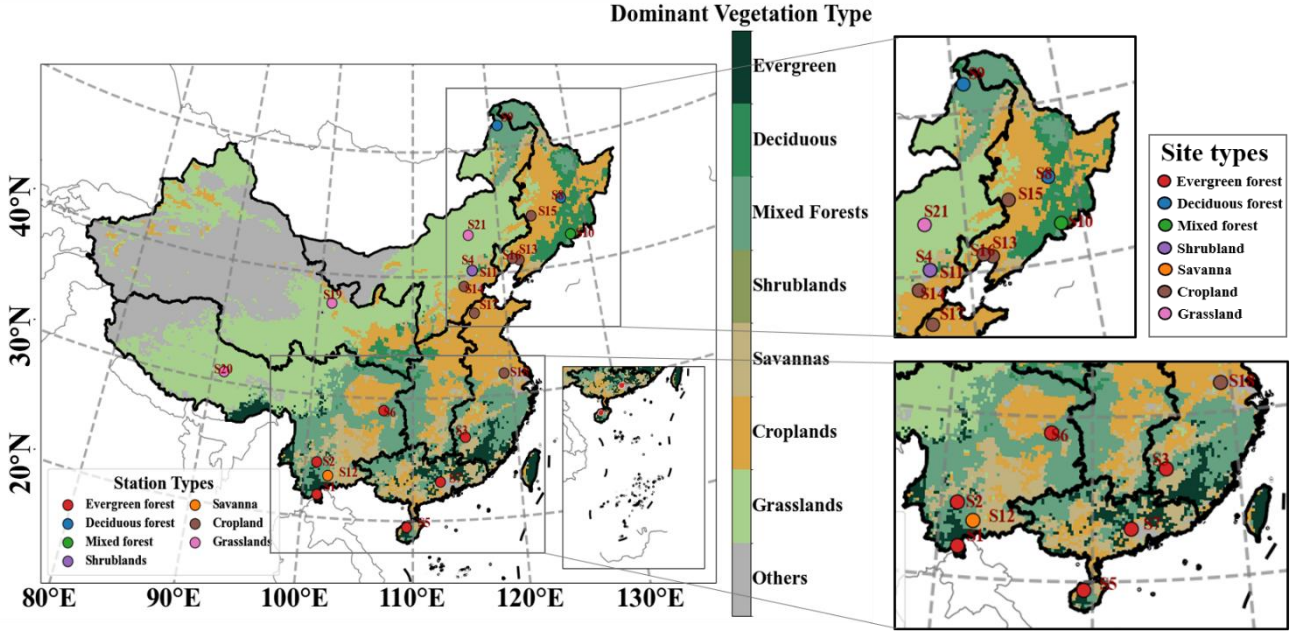


Figure 1. **Study domain and dominate vegetation types.** Circles indicate ground sites for in-situ eddy covariance measurements.

https://doi.org/10.5194/egusphere-2026-6317
Preprint. Discussion started: 11 November 2026
© Author(s) 2026. CC BY 4.0 License.

2.2 WRF-VPRM model

Gridded NEP data were simulated by coupling the WRF-VPRM model, where major model parameters were calibrated using the aforementioned in-situ measurements to improve simulation accuracy. The WRF model is a mesoscale meteorological model that simulates atmospheric processes and provides high-resolution meteorological fields for regional applications. This study employed WRF v4.5 to provide meteorological fields to drive VPRM model simulation. VPRM is a light-use-efficiency (LUE) based diagnostic model (Mahadevan et al., 2008). It decomposes net ecosystem exchange (NEE) into a light-driven GEE component and a temperature-driven ER component (Ahmadov et al., 2007; Xiao et al., 2004) Eq. (1). NEP was calculated as the negative value of NEE Eq. (2). For RES, VPRM assumes a linear response to surface temperature and distinguishes vegetation types using respiration sensitivity parameters (α and β). For GEE process, VPRM uses the half-saturation parameter (PAR_0) and light-use efficiency (λ) to represent photosynthetic carbon uptake (Mahadevan et al., 2008). This parsimonious structure facilitates calibration of key parameters with in-situ measurements (Park et al., 2018).

$$NEE = GEE + ER \tag{1}$$

$$NEP = -NEE \tag{2}$$

$$ER = \alpha \cdot T + \beta \tag{3}$$

$$GEE = -\lambda \cdot T_{scale} \cdot W_{scale} \cdot P_{scale} \cdot \frac{1}{1 + \frac{PAR}{PAR_0}} \cdot EVI \cdot PAR \tag{4}$$

$$T_{scale} = \frac{(T - T_{min}) \cdot (T - T_{max})}{[(T - T_{min}) \cdot (T - T_{max})] - (T - T_{opt})^2} \tag{5}$$

$$W_{scale} = \frac{1 + LSWI}{1 + LSWI_{max}} \tag{6}$$

$$P_{scale} = \frac{1 + LSWI}{2} \tag{7}$$

Where T denotes 2m air temperature (T_2); T_{scale}, W_{scale}, and P_{scale} are the scalars representing temperature limitation, moisture stress, and phenology, respectively; PAR is photosynthetically active radiation, and PAR_0 is the half-saturation constant; T_{min}, T_{max} and T_{opt} are minimum, maximum and optimal air temperature for photosynthetic activities, respectively; T_{scale} is set to zero when temperature is below T_{min}; LSWI is the land surface water index, VPRM uses first-order approximations to represent the seasonal variations in W_{scale} and P_{scale}. $LSWI_{max}$ is the maximum LSWI within the growing season for vegetation. Parameters α, β, λ, and PAR_0 are vegetation-type–specific values. This study used the key parameters (α, β, λ) from Li et al. (2020) as default set-up and calibrated the values with in-situ measurements.

https://doi.org/10.5194/egusphere-2026-6317
Preprint. Discussion started: 11 November 2026
© Author(s) 2026. CC BY 4.0 License.

2.2.1 Model set-up

The modeling domain covers China mainland at a horizontal resolution of 20×20 km (Fig. 1). The model configuration includes 47 vertical layers, with the model top set at 10 hPa. Meteorological initial and boundary conditions were obtained from the Final Analysis (FNL) data. This dataset was produced by the National Center for Environmental Prediction (NCEP) and provides data every 6 hours at a spatial resolution of 1°×1°. Key atmospheric variables from the FNL dataset were used to initialize the model and specify lateral boundary conditions. These variables include temperature, pressure, and relative humidity. Using FNL data for initialization and boundary forcing improves the reliability of model simulations. The model uses several physical parameterization schemes. These include the Noah land surface model, the Morrison microphysics scheme, the Rapid Radiative Transfer Model for GCMs (RRTMG) for shortwave and longwave radiation, the Grell-3 cumulus parameterization, and the Yonsei University (YSU) planetary boundary layer scheme. To better represent large-scale atmospheric forcing and improve the simulation of meteorological fields, spectral nudging was applied to constrain the model toward reanalysis data. Background and initial CO_2 concentrations were obtained from the Copernicus Atmosphere Monitoring Service global greenhouse gas reanalysis (EGG4) monthly mean fields. Land-use and land-cover inputs were derived from MODIS MCD12Q1. EVI and LSWI were calculated from MODIS MOD09A1 v6.1 products.

2.2.2 Model evaluation and calibration

The default parameterization captured the seasonal patterns of both GEE and ER fluxes but exhibited systematic biases across vegetation types (Fig. S1), particularly at southern and subtropical sites. To improve the model performance, we calibrated two key parameters that dominate the magnitude of GEE and ER fluxes in the VPRM model. For the respiration formulation, we calibrated parameter α, which determines the response of ER fluxes to temperature changes. For the photosynthesis process, we adjusted parameter λ, which defines the light-use efficiency of vegetation. Calibration was performed independently for each vegetation type using the least squares method coupled with a genetic algorithm to avoid local optima. The objective function was defined to minimize the root mean square error (RMSE) and maximize the coefficient of determination (R^2) between simulated and observed GEE and ER fluxes. The calibrated parameters were compared with those in default model in Table S3. The calibration has substantially improved agreement with in-situ observations compared to the default parameterization (Fig. S1). The calibrated model achieved much higher correlation coefficients for both GEE (R^2 = 0.61–0.90) and ER (R^2 = 0.31–0.98), with slopes closer to 1.0 and reduced mean biases. The modelled NEP-temperature relationships were also broadly consistent with site-based observations (Fig. S2).

2.3 XGBoost-SHAP analysis

2.3.1 Extreme Gradient Boosting (XGBoost)

XGBoost model was employed to establish quantitative relationships between gridded carbon fluxes (i.e., GEE and ER as dependent variables) from calibrated WRF-VPRM and environmental drivers (Chen and Guestrin, 2016). We initially

https://doi.org/10.5194/egusphere-2026-6317
Preprint. Discussion started: 11 November 2026
© Author(s) 2026. CC BY 4.0 License.

compiled 36 candidate predictive variables encompassing vegetation status, climatic forcing, and geographic and soil attributes (Table S4). To eliminate multicollinearity and improve model interpretability, the variance inflation factor (VIF) was applied for feature screening, with a threshold of VIF < 10 adopted to remove highly redundant predictors. We retained 11 core predictors for final modeling (Table S5). Separate XGBoost models were constructed for GEE and ER to resolve their distinct driving mechanisms. A total of 289,668 gridded sample pairs were used for model training and validation. The full dataset was randomly partitioned into an 80% training subset and a 20% independent testing subset. Model hyperparameters were optimized via 10-fold cross-validation to avoid overfitting. The optimal hyperparameters are listed in Table S6. The optimized XGBoost models achieved high predictive accuracy on the independent test dataset, with R^2 values of 0.96 for GEE and 0.97 for ER (Fig. S3), demonstrating that the selected driver variables can reliably capture the spatial and temporal variability of terrestrial carbon fluxes across China.

2.3.2 SHAP model

We adopted the SHAP model (Dwivedi et al., 2023; Lundberg and Lee, 2017) to quantify the marginal contributions of individual drivers (Merabet et al., 2025) and identify the dominant climatic controls on GEE and ER and characterize their nonlinear responses to rising air temperature. SHAP summary plots showed that near-surface air temperature contributed 27% of total SHapley Additive exPlanations (SHAP)-based explanatory power for GEE and 59% for ER (Fig. S4). Land Use and Land Cover (LULC), Enhanced Vegetation Index (EVI), and precipitation followed as secondary controls. SHAP dependence plots were then adopted to explicitly visualize the continuous response curves of GEE and ER along temperature gradients, revealing how temperature fluctuations regulate terrestrial carbon assimilation and respiration processes across diverse vegetation types.

2.4 Prediction of future changes in NEP

2.4.1 Future climate and LULC scenarios

Future spatiotemporal changes in terrestrial NEP were predicted using the XGBoost model driven by dynamically projected climatic factors and LULC data under three core SSP scenarios, including SSP126, SSP245, and SSP585. To quantitatively disentangle the independent and interactive effects of climate change and LULC transformation on carbon sink variations, three comparative simulation experiments were designed in this study (Table 1). The baseline scenario (Base) adopted 2020 WRF-VPRM climate and LULC datasets to represent the contemporary NEP status in 2020 and was used for model evaluation, contemporary carbon sink estimation, and the warming sensitivity experiment. For future SSP projections, NEP anomalies were calculated relative to the 2020 value to ensure consistency with the future climate and LULC datasets. The full future scenario (Climate and Land-use) utilized scenario-specific projected climate and LULC data to simulate NEP dynamics at five-year intervals from 2020 to 2060 across the three SSP frameworks. A control scenario was further established for contribution separation: the climate-only scenario incorporated future climate projections while fixing LULC

https://doi.org/10.5194/egusphere-2026-6317
Preprint. Discussion started: 11 November 2026
© Author(s) 2026. CC BY 4.0 License.

patterns at the 2020 baseline level. Specifically, the pure effect of climate change was quantified as the NEP difference between the Climate-only and Base scenario, and the synergistic combined effect of climate and LULC changes was determined by the discrepancy between Climate and land-use and Base results.

Table 1 Base and future scenarios

Scenarios	Climate data	LULC data	Simulation Year
Base	2020	2020	2020
Climate and land-use	SSP126, 245 and 585	SSP126, 245, 585	Every five years from 2020 to 2060
Climate-only	SSP126, 245 and 585	2020	

2.4.2 Future climate data of temperature

Three representative SSP scenarios covering low, moderate, and high radiative forcing levels (SSP126, SSP245, and SSP585) were adopted to capture a full range of future climate change trajectories (Gidden et al., 2019). Future near-surface temperature values were derived from a high-resolution downscaled Coupled Model Intercomparison Project Phase 6 (CMIP6) multi-model ensemble product developed by Zhang et al. (2025a). This dataset was generated using a Residual Channel Attention Network (RCAN) deep learning algorithm, which downscaled coarse-resolution CMIP6 global climate outputs by learning high-precision spatiotemporal features from 10 km ERA5-Land reanalysis data. The ensemble mean results from five mainstream CMIP6 models were adopted to reduce single-model uncertainty and improve projection reliability. To match the 20 km spatial resolution of the calibrated WRF-VPRM and XGBoost modeling framework, the original 10 km climate dataset was resampled using the nearest-neighbor interpolation algorithm in Python (v3.11.11). Daily temperature records were aggregated into monthly scale values to align with the temporal resolution of historical carbon flux simulations. The monthly mean temperature values were finally adopted as core climatic predictive variables for future NEP dynamic projections.

2.4.3 Future LULC and EVI data

Future LULC trajectories were obtained from the downscaled Land Use Harmonization 2 (LUH2) dataset. The original 0.25° LUH2 product was spatially refined to a 1 km resolution in a previous study by Hou et al. (2022), providing continuous future projections of major land cover types (including forest, cropland, grassland, and urban land) across China (Shen et al., 2024; Krause et al., 2022). The scenario-based dynamic LULC data were extracted and converted into the LU_INDEX variable required for XGBoost future predictions (Fig. S5).

To generate vegetation forcing data that dynamically couples with future climate and LULC changes, we constructed independent statistical extrapolation models to predict the eight vegetation-specific EVI components (EVI0–EVI7) for future scenario simulations. A random forest algorithm was employed for each EVI component, with individual EVI values set as dependent variables. The predictive drivers included monthly near-surface air temperature, accumulated precipitation, seasonal month, LU_INDEX, and spatial grid coordinates (Grid_X, Grid_Y).

https://doi.org/10.5194/egusphere-2026-6317
Preprint. Discussion started: 11 November 2026
© Author(s) 2026. CC BY 4.0 License.

Considering the strong temporal autocorrelation of monthly EVI observations within individual grid cells, a grouped spatial cross-validation strategy was applied to ensure conservative and robust model evaluation. All grid cells were grouped by spatial coordinates and randomly divided into an 80% training dataset and a 20% independent testing dataset at the grid level. The established EVI extrapolation models exhibited excellent performance across all vegetation types, with testing R^2 values ranging from 0.70 to 0.95 (Fig. S6). The generated monthly EVI0–EVI7 datasets under the three future SSP scenarios were used as dynamic vegetation input variables for subsequent future NEP projections.

3 Results

3.1 Site-observed nonlinear relationships between NEP and temperature

Air temperature, solar radiation, precipitation, and soil moisture are widely recognized as key climatic drivers regulating terrestrial ecosystem NEP (Tang et al., 2021; Wang et al., 2023a). In this study, we focus specifically on the NEP–temperature relationship, given its strong collinearity with net solar radiation (R = 0.85) and multi-layer soil temperature (R = 0.82–0.94) across the study region (Fig. S7). This high collinearity means air temperature can broadly represent combined thermal forcing from related co-varying variables.

In-situ observations reveal a pronounced nonlinear NEP–temperature relationship, with clear differences in magnitude and shape among vegetation types (Fig. 2). Forest ecosystems (evergreen, deciduous, and mixed forests, Fig. 2a-c) exhibited the strongest temperature sensitivity and consistently functioned as net carbon sinks. Their NEP was near zero or slightly negative under low temperatures (<0°C), increased continuously at moderate temperatures (0–20°C), and declined above this range. This weakening carbon sink strength at high temperatures was driven by two concurrent processes: a slowdown in the temperature-induced increase of GEE (carbon uptake), paired with a persistent and linear rise in ER (carbon release). Croplands showed a distinct pattern, acting as carbon sources at low temperatures (<10°C), with NEP rising sharply around 10–20 °C to cross zero and become a carbon sink. At temperatures above 20°C, however, cropland GEE was increasingly inhibited, leading to a gradual decline in NEP. In contrast, savannas, grasslands, and shrublands showed much weaker temperature sensitivity. Savanna NEP remained near zero across the entire observed temperature range, indicating no clear sink or source behavior. Grasslands and shrublands were weak carbon sources at temperatures below 0°C, with only small increases in NEP as temperatures rose, followed by modest declines after crossing vegetation-specific statistical turning points. Note that parts of the high-temperature response curves in Fig. 2 rely on statistical extrapolation where in-situ flux observations are sparse (see Methods). Across all vegetation types, the site-scale data confirmed a consistent temperature threshold pattern with statistical turning points.

Site-scale data show that NEP across vegetation types displays distinct statistical turning points, which turned out a board range of potential temperature threshold for NEP, ranging from 15-25°C (Fig. 2h). The in-situ measurements derived NEP-temperature response depends largely on site-selection, vegetation-composition, and analytical-methods, which caused substantial differences among this study and previous findings. For example, Huang et al. (2019) derived ecosystem-level

https://doi.org/10.5194/egusphere-2026-6317
Preprint. Discussion started: 11 November 2026
© Author(s) 2026. CC BY 4.0 License.

statistical turning points for GPP of 23±6 ℃ globally and ~18–24 ℃ for China, noting that GPP-derived features do not directly equate to NEP responses modulated by ecosystem respiration. Xu et al. (2025) reported NEP increases from −5 to 17 ℃ in boreal and temperate regions, followed by a slight decline. Fu et al. (2023) found a similar trend, with NEP rising up to 16.4 ℃ before decreasing. Indeed, our vegetation-specific analysis revealed substantial heterogeneity. Most forest types showed a single peak at 15–20 ℃, grasslands peaked near 10 ℃, savannas at 25–30 ℃, and evergreen forests exhibited a bimodal pattern with peaks at 5–10 ℃ and 25 ℃. Such variability underscores the need to move beyond site-level observations to capture the full range of regional conditions across China's diverse climate zones and vegetation types, motivating our subsequent regional-scale modelling analysis.

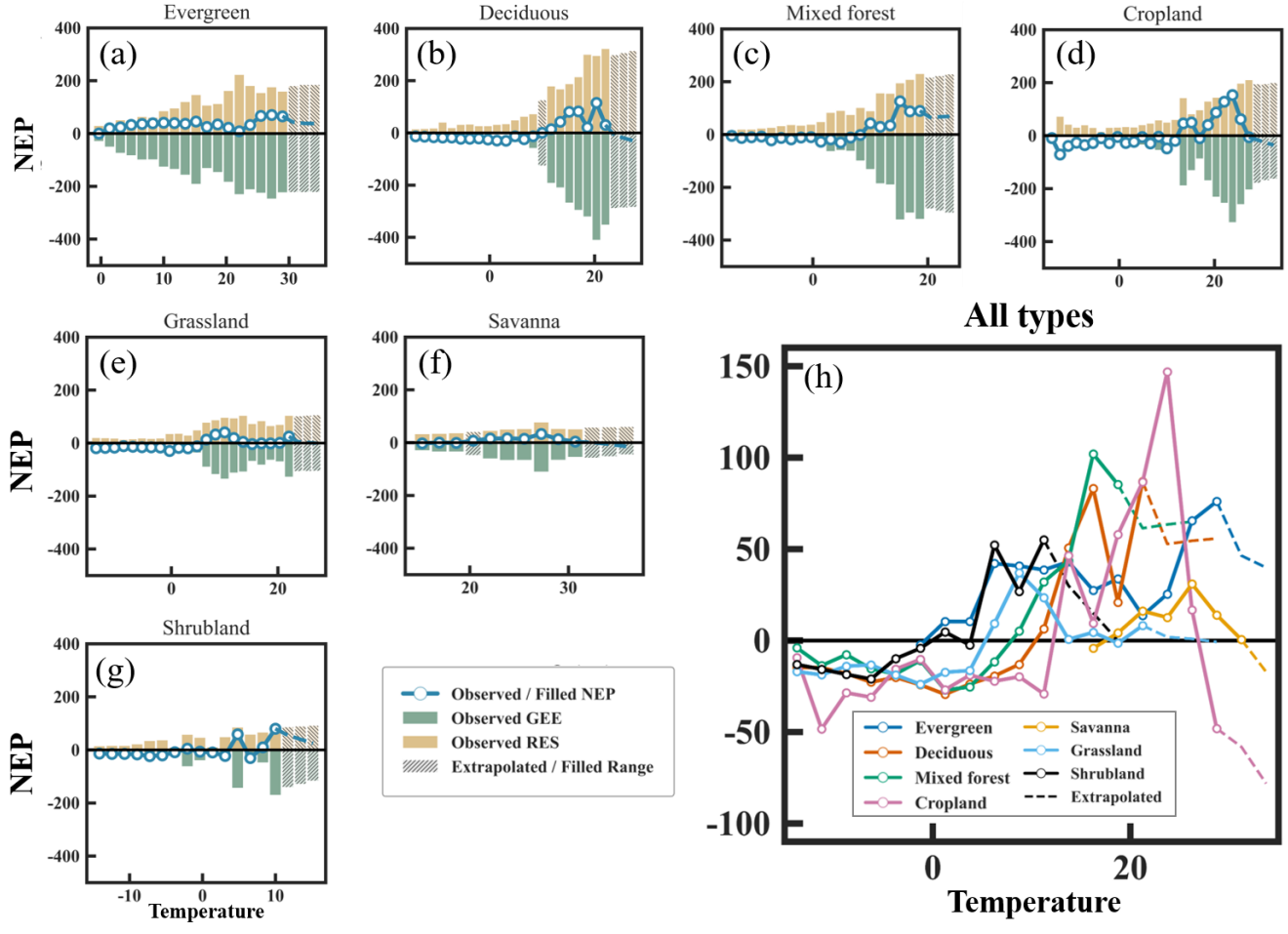


Fig. 2. Observed relationships between carbon fluxes (NEP, GEE and ER) and temperature at seven vegetation types. The blocks in solid line indicate data from in-situ observations and those in dashed line came from external interpolation (See Methods).

https://doi.org/10.5194/egusphere-2026-6317
Preprint. Discussion started: 11 November 2026
© Author(s) 2026. CC BY 4.0 License.

3.2 Threshold-dependent pattern between NEP and temperature at regional scale

To extend site-scale findings to the regional scale, we first simulated GEE and ER fluxes across China using the calibrated WRF-VPRM model. Model performance against in-situ measurements demonstrated reliable performance in reproducing both magnitudes and seasonal variations of carbon fluxes (Fig. S1). The model also well reproduced vegetation-specific NEP–temperature relationships across seven major plant functional types at the site level (Fig. S2), providing a solid basis for regional-scale analysis. Site-scale observations reveal distinct unimodal NEP–temperature curves for individual vegetation types (Fig. 2). When aggregated to regional grids, the composite curve exhibits a more complex segmented nonlinear pattern (Fig. 3). This scale-dependent divergence indicates that site-derived thermal response curves cannot be directly extrapolated to regional carbon budgets, because the geographical distribution of vegetation types reshapes the emergent macroscale carbon–temperature relationship.

Point density distributions represent the dominant temperature regimes that each vegetation type currently experiences. The degree of mismatch between the modal temperature (most frequent ambient temperature) and the statistical NEP peak temperature (black lines) strongly differs across plant functional types, leading to divergent warming responses. For evergreen forests (Fig. 3a), the modal temperature (~15 °C) closely matches their NEP peak, implying that most evergreen forest ecosystems currently operate near their statistical thermal optimum for carbon sequestration. Consequently, future warming will shift these systems to the declining branch of the response curve and reduce carbon sink capacity. In contrast, savanna ecosystems are mainly distributed at 18–20 °C (Fig. 3f), which is lower than their NEP peak temperature (~22 °C), indicating that moderate warming may further enhance savanna carbon sequestration. Overall, most vegetation types show declining NEP once temperatures exceed their type-specific optimal thermal ranges.

The regional aggregated NEP–temperature relationship exhibits clear segmented nonlinearity. From −10 to 0 °C, NEP increases rapidly with warming, reflecting strong temperature limitation on carbon sequestration under cold conditions. The temperature sensitivity substantially weakens from 0 to 18 °C, forming a buffered response range at the regional scale, where carbon sink capacity remains relatively stable despite ongoing temperature fluctuations. Notably, this macroscopic buffer effect conceals substantial functional heterogeneity among vegetation types. At temperatures above 22 °C, regional NEP decreases sharply, indicating widespread thermal suppression of terrestrial carbon sequestration under high-temperature conditions. These static spatial patterns of NEP-temperature relationships reveal type-specific thermal constraints on carbon sequestration. To further quantify how incremental warming alters terrestrial carbon sink strength, we conducted targeted temperature sensitivity experiments, as described in the following section. These scale-dependent and type-specific thermal responses improve our understanding of heterogeneous terrestrial carbon cycle feedbacks under ongoing climate warming.

https://doi.org/10.5194/egusphere-2026-6317
Preprint. Discussion started: 11 November 2026
© Author(s) 2026. CC BY 4.0 License.

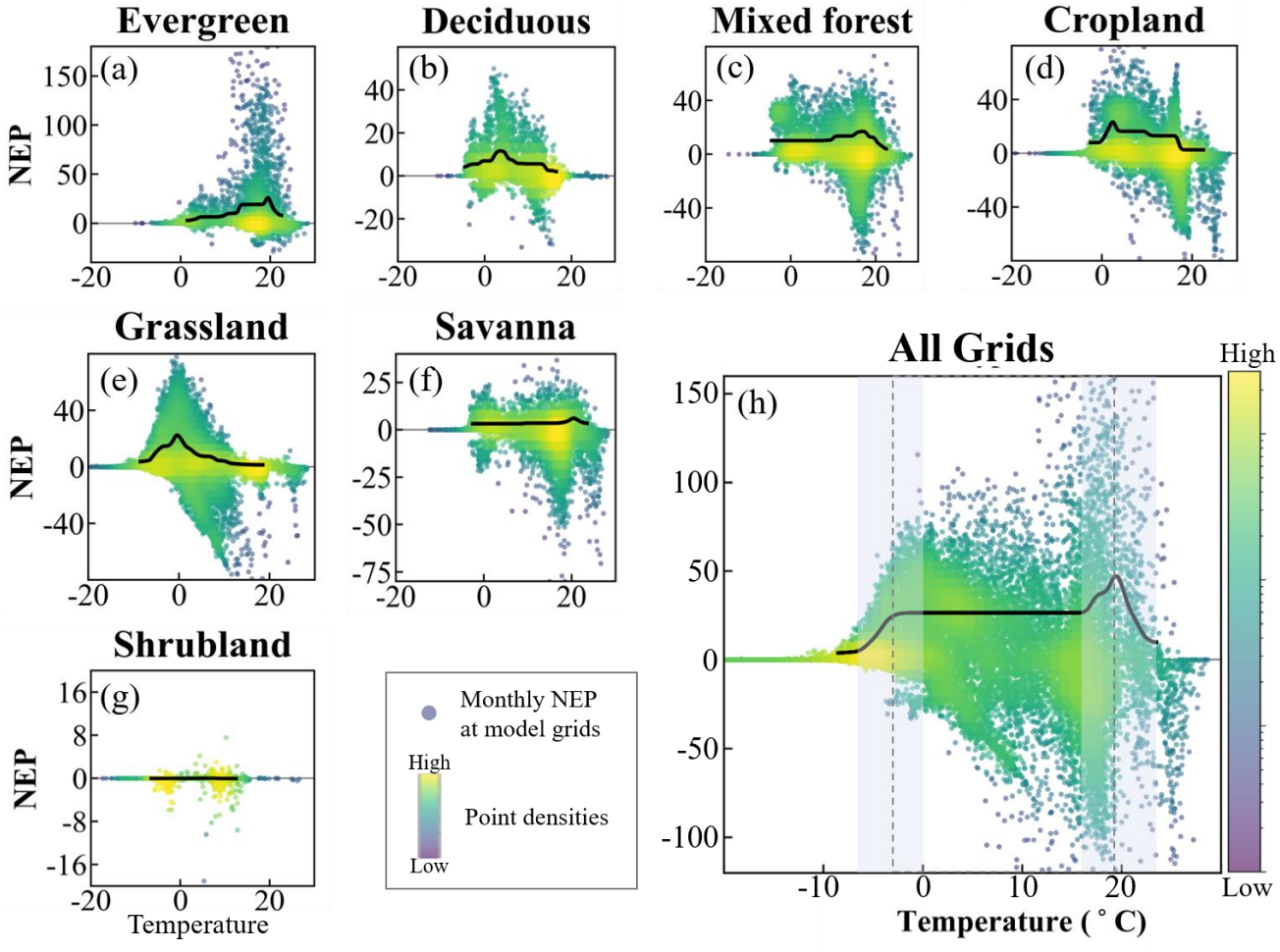


Fig. 3 Modelled relationships between NEP and temperature at seven vegetation types (a-g) and for all types (h). Each point denotes the NEP results of a model grid and the colors indicate point densities.

3.3 Sensitivity of regional NEP to temperature increase

To assess the sensitivity of China's terrestrial carbon sink to warming, we conducted a controlled warming experiment imposing a uniform +0.5 ℃ rise in near-surface air temperature, while holding other environmental drivers (LULC, precipitation, EVI) fixed at the 2020 baseline level. Nationally, this warming perturbation reduces total NEP by 0.17 Pg C yr^{-1}, equivalent to a 31% loss of terrestrial carbon sink capacity. Spatially, pronounced declines in NEP are widespread across eastern China, whereas limited positive NEP anomalies appear in high-elevation regions of the southern Tibetan Plateau (Fig. 4a).

These spatial disparities arise from divergent vegetation-specific warming sensitivities (Fig. 4b). Under baseline conditions, forest ecosystems (evergreen, deciduous, and mixed forests) dominate national sink strength, which

https://doi.org/10.5194/egusphere-2026-6317
Preprint. Discussion started: 11 November 2026
© Author(s) 2026. CC BY 4.0 License.

contribute >80% of total NEP while occupying only 14% of China's land area. Evergreen forests alone contribute 45% of the total terrestrial sink, and mixed forests contribute an additional 25%. Under the +0.5 ℃ warming perturbation, deciduous forests (mainly distributed across northeast China) show a moderate 22% NEP reduction, and mixed forests (distributed in southern China) show a 40% reduction. By contrast, evergreen forests retain the most stable sink capacity with only a 6% NEP decline. Croplands showed the largest relative sink loss among all vegetation categories (77%), driving large sink declines in eastern China. Grasslands, distributed across northwestern and northeastern China, contribute 16% of national NEP and show a 28% reduction under warming.

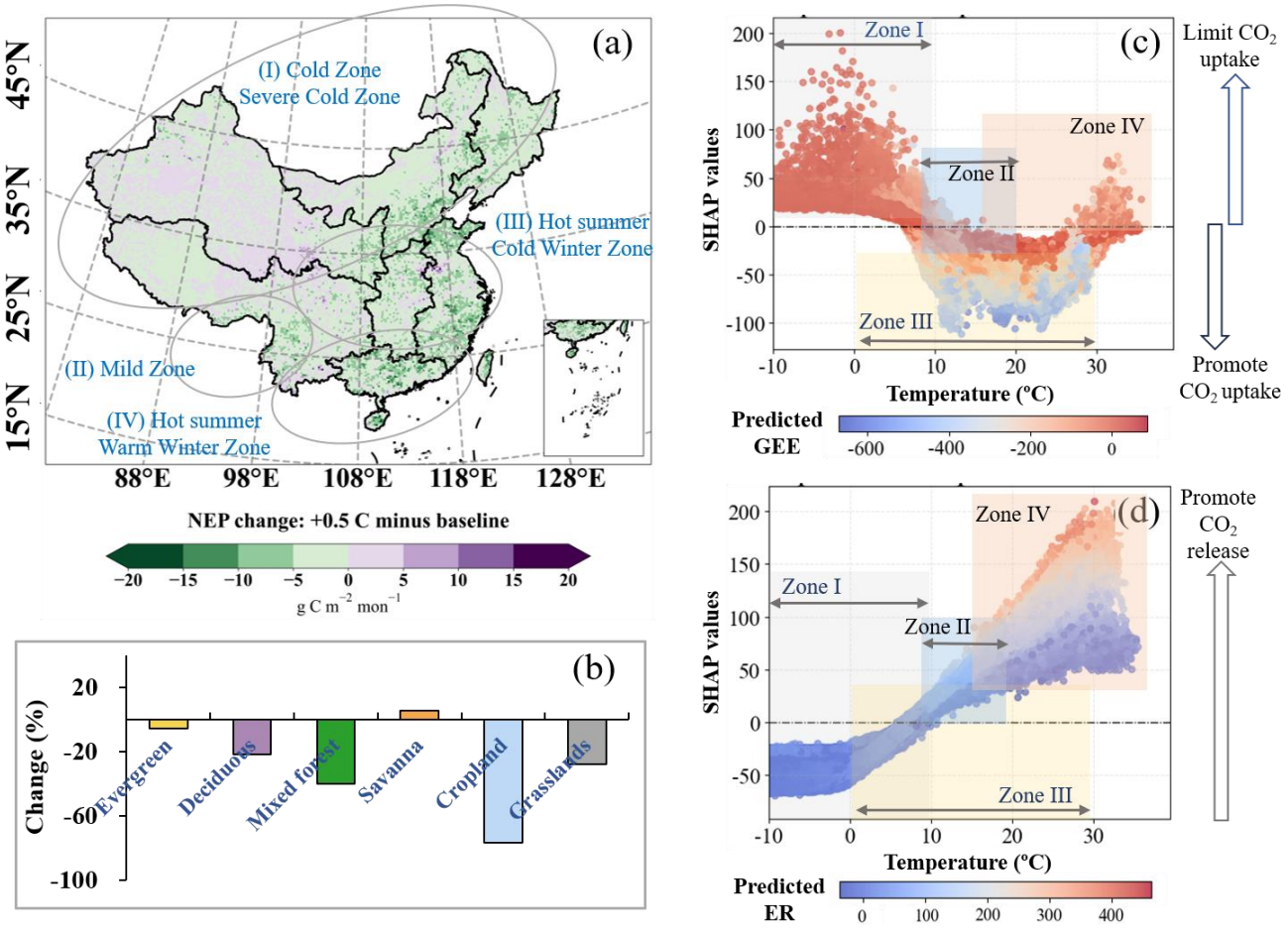
SHAP dependence plots further reveal piecewise and heterogeneous temperature controls over GEE and ER across climatic zones (Fig. 4c,d). For GEE (Fig. 4c), vertical SHAP values quantify the marginal effect of temperature on modelled gross photosynthesis. Our modelling framework adopts a sign convention where negative GEE values represent photosynthetic CO_2 uptake and therefore more negative GEE corresponds to stronger carbon fixation. A positive SHAP value indicates warming shifts GEE toward zero and limits CO_2 uptake, while a negative SHAP value means warming makes GEE more negative and promotes CO_2 uptake. Temperature had a weak positive contribution below 0 ℃, as low temperatures limited photosynthetic activity. Between 5 and 25℃, rising temperature strongly promoted GEE (large negative SHAP values), reflecting alleviation of thermal limitation and enhanced photosynthetic efficiency. The promotion effects are weaker above 25℃ and turned negative after 30℃. At this stage, temperature exceeds the response-derived photosynthetic optimum and warming tends to suppress plant photosynthesis (Niu et al., 2012; Yvon-Durocher et al., 2010). In contrast, ER (Fig. 4d) exhibited a monotonic-positive response to temperature across the entire range (Wang et al., 2023b).

The contrasting thermal responses of GEE and ER jointly shape net NEP changes across climatic zones. In Zone I (cold and severe cold zone, temperature < 10°C), warming limits photosynthetic CO_2 uptake while markedly accelerating ER, resulting in a net reduction of NEP. In Zone II (mild zone with a narrow temperature range between 10℃ and 20℃), GEE responses diverge among ecosystems, yet ER rises rapidly with temperature, leading to overall minor sink weakening. Zone III (hot summer and cold winter zone with a board temperature range between 0 and 30°C) is dominated by high-GEE ecosystems where warming generally enhances photosynthesis. However, the concurrent strong rise in ER outweighs photosynthetic gains and reduces NEP. In Zone IV (hot summer and warm winter zone, >15°C), warming prohibits photosynthetic CO_2 uptake, together with the monotonic rise in ER, causing large net NEP decline. This effect is particularly pronounced in tropical and subtropical regions, where growing-season temperatures are already close to ecosystem-scale statistical thermal optima (Corlett, 2011; Doughty and Goulden, 2008). The vegetation-specific and zone-dependent NEP sensitivity shown here aligns with the heterogeneous NEP–temperature statistical relationships identified in the preceding analysis. Ecosystems whose baseline temperature sit close to their photosynthetic optimum exhibit larger sink losses under warming. We note this is an idealized single-factor warming experiment and real-world future climate change will alter precipitation and vegetation dynamics simultaneously, which may modify the magnitude of sink weakening.

Our modelled sink response to warming is broadly consistent with previous large-scale terrestrial carbon cycle assessments, though the magnitude of sensitivity varies across published work. Early studies showed a very large sensitivity

https://doi.org/10.5194/egusphere-2026-6317
Preprint. Discussion started: 11 November 2026
© Author(s) 2026. CC BY 4.0 License.

range among different models. Berthelot et al. (2005) analyzed outputs from 14 global models and calculated the impact of temperature change on NEP using ΔNEP/ΔT. All models yielded negative values, showing that temperature increases tend to suppress NEP, with response values ranging from -6.7 to -73.9 PgC °C^{-1} (on average −47 PgC °C^{-1}). Friedlingstein et al. (2006) summarized the results of 11 global models and the average response ranged from -20 to -177 PgC °C^{-1}, on average −79 PgC °C^{-1}. Piao et al. (2013) evaluated the sensitivity of global net biome productivity under warming using outputs from 10 process-based terrestrial biosphere models, and found good inter-model agreement of −3±1.5 PgC °C^{-1} for global totals. A recent study (Fernández-Martínez et al., 2019) used atmospheric inversion and TREDY and estimated global NEP-temperature sensitivity of −0.5 to −1.1 PgC per degree of temperature increase. Assuming China accounts for 13-18% of global terrestrial NEP (Friedlingstein et al., 2006), the corresponding sensitivity for China would be approximately −0.13 to −0.81 PgC °C^{-1}. In our +0.5 °C sensitivity experiment, the NEP reduction of 0.17 PgC yr^{-1}, corresponds to a temperature sensitivity of approximately −0.34 PgC °C^{-1}. Our estimated temperature sensitivity for China falls within the wide range reported by regional subsets of global model outputs. Direct cross-study comparison remains complicated, however, due to divergent experimental set-ups, variable definitions and spatial aggregation strategies across previous studies.



https://doi.org/10.5194/egusphere-2026-6317
Preprint. Discussion started: 11 November 2026
© Author(s) 2026. CC BY 4.0 License.

Figure 4. Spatial, vegetation-type and mechanistic responses of terrestrial carbon fluxes under the uniform +0.5 °C warming experiment. (a) Spatial distribution of NEP changes (ΔNEP, unit: g C m^{-2} mon^{-1}) across four climatic zones of China. (b) Relative percentage changes in NEP for major vegetation types under warming. SHAP dependence plots showing temperature effects on (c) GEE and (d) ER. Background shading denotes the four climatic zones. In panel (c), negative modelled GEE represents photosynthetic CO_2 uptake, and more negative values indicate stronger carbon fixation. Positive SHAP values reduce CO_2 uptake, while negative SHAP values enhance CO_2 uptake. In panel (d), positive ER values denote carbon release, and higher SHAP values indicate stronger promotion of CO_2 release by rising temperature. Scatter colour corresponds to predicted flux magnitude. The temperature range of four climatic zones (Zone I–IV) were defined based on regional baseline temperature conditions (Fig. S8).

3.4 Temperature-induced weakening of carbon sink potential

Future NEP variations under three SSP scenarios were quantified against the 2020 baseline representing impacts of climate change (Fig. 5, grey line) and combined impacts of climate change and land cover conversion (Fig. 5, green line). All percentage changes reported hereafter are relative to this SSP-driven 2020 reference state. This 2020 baseline was used only for future trajectory comparisons, whereas the 2020 WRF-VPRM baseline was used for contemporary NEP estimation and the warming sensitivity experiment. Temperature rises remained limited below 1 °C across all three SSP scenarios by 2030, triggering only mild national-scale NEP fluctuations. Considerable divergence emerged by 2060, with national-mean air temperature increasing by 0.6 °C, 1.1 °C and 1.7 °C under SSP1-26, SSP2-45 and SSP5-85, respectively (relative to the scenario-specific 2020 baseline). These magnitudes of warming drove dramatic declines in national NEP, with relative changes reaching −24%, −27% and −56% under SSP1-26, SSP2-45 and SSP5-85, respectively. Comparing climate-only (grey line) and climate-and-land-use (green line) trajectories reveals that vegetation and land cover dynamics partially buffer warming-induced NEP reduction across all three SSPs (discussed in next section).

Spatially (Fig. 6), changes in carbon-sink capacity in year 2060 displayed pronounced spatial heterogeneity under future warming in 2060, with the most pronounced divergent responses observed under the high-emission SSP5-85 scenario (Fig. 6g). Eastern China became the dominant hotspot of future carbon sink loss, especially within the latitudinal bands of 15–25° N and 35–45° N (Fig. 6e,h). Such spatial variation largely coincides with the warming response characteristics obtained from the 0.5 °C sensitivity test (Fig. 4a). By contrast, the southern Tibetan Plateau and parts of Northeast China exhibited clear increasing trends in NEP (Fig. 6d, R1-R3). These divergent responses will be addressed in the following section.

Vegetation types exhibited strongly divergent relative changes in NEP by 2060 (Fig. 6c,f,i), with contrasting sensitivity across SSP emission pathways. Under SSP1-2.6, national NEP changes remained modest for forests (−7%) relative to the 2020 baseline. The overall reduction in terrestrial carbon sink was primarily driven by croplands (−20%) and grasslands (−105%) with pronounced declines in NEP. For SSP2-4.5, most vegetation groups except shrublands showed reduced NEP. Forests experienced an 18% reduction, close to the national mean decrease (−27%). Mixed forests and grasslands showed the largest relative losses, at −40% and −44%, respectively. Under the high-emission SSP5-8.5 scenario, all vegetation types underwent NEP declines, leading to a total national NEP reduction of 56%. Forest carbon sinks decreased by 23%, while

https://doi.org/10.5194/egusphere-2026-6317
Preprint. Discussion started: 11 November 2026
© Author(s) 2026. CC BY 4.0 License.

grasslands displayed the most severe relative loss (−170%). This large negative percentage value indicates a reversal from net carbon sink to net carbon source for grasslands. Results for shrublands should be interpreted with caution due to limited observational constraints and high uncertainty. Across the three climate scenarios, grasslands consistently showed the highest proportional vulnerability to warming, while forests exhibited comparatively smaller relative NEP losses. These divergent vegetation-specific responses are consistent with the scale-dependent thermal sensitivities derived from our controlled warming experiment, highlighting the heterogeneous vulnerability of terrestrial carbon sequestration across plant functional types under climate warming.

Overall, climate warming exerted pervasive negative impacts on future terrestrial NEP, and this inhibitory effect intensified with rising emission levels, following the gradient SSP5-85 > SSP2-45 > SSP1-26. The inhibitory effect remained weak in the near-term, yet was strongly amplified after ~2040, yielding NEP reductions ranging from 26% to 56% depending on the climate scenario. Warming suppresses carbon assimilation in mid-low-latitude regions approaching the statistical thermal optimum (Huang et al., 2019), while moderate temperature increases relieve low-temperature constraints in high-altitude and high-latitude zones, generating clear spatial differentiation in terrestrial carbon-sink evolution across China.

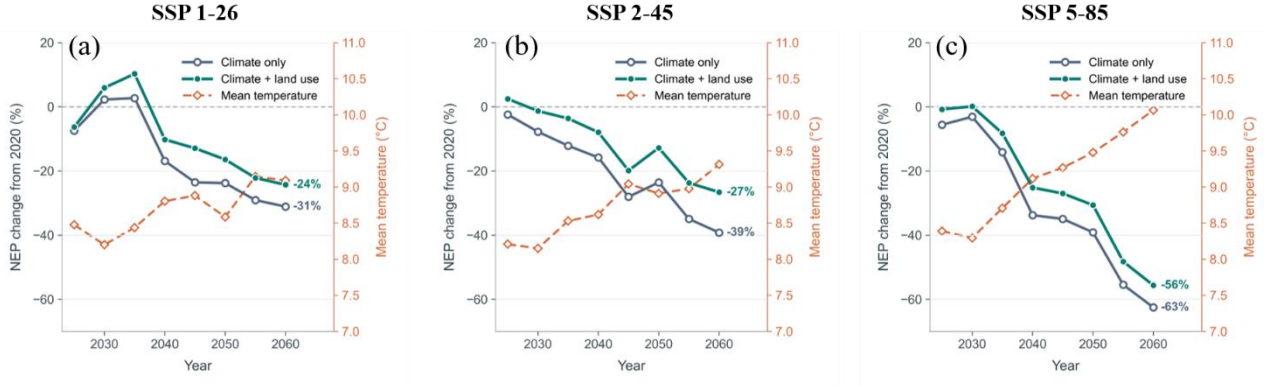


Figure 5 Temporal percentage changes of national average NEP anomalies from 2025 to 2060 under SSP 1-26, SSP 2-45 and SSP 5-85. Orange lines denote temperature changes, grey lines denote NEP under climate change only, green lines denote NEP under climate and land-use changes.

https://doi.org/10.5194/egusphere-2026-6317
Preprint. Discussion started: 11 November 2026
© Author(s) 2026. CC BY 4.0 License.

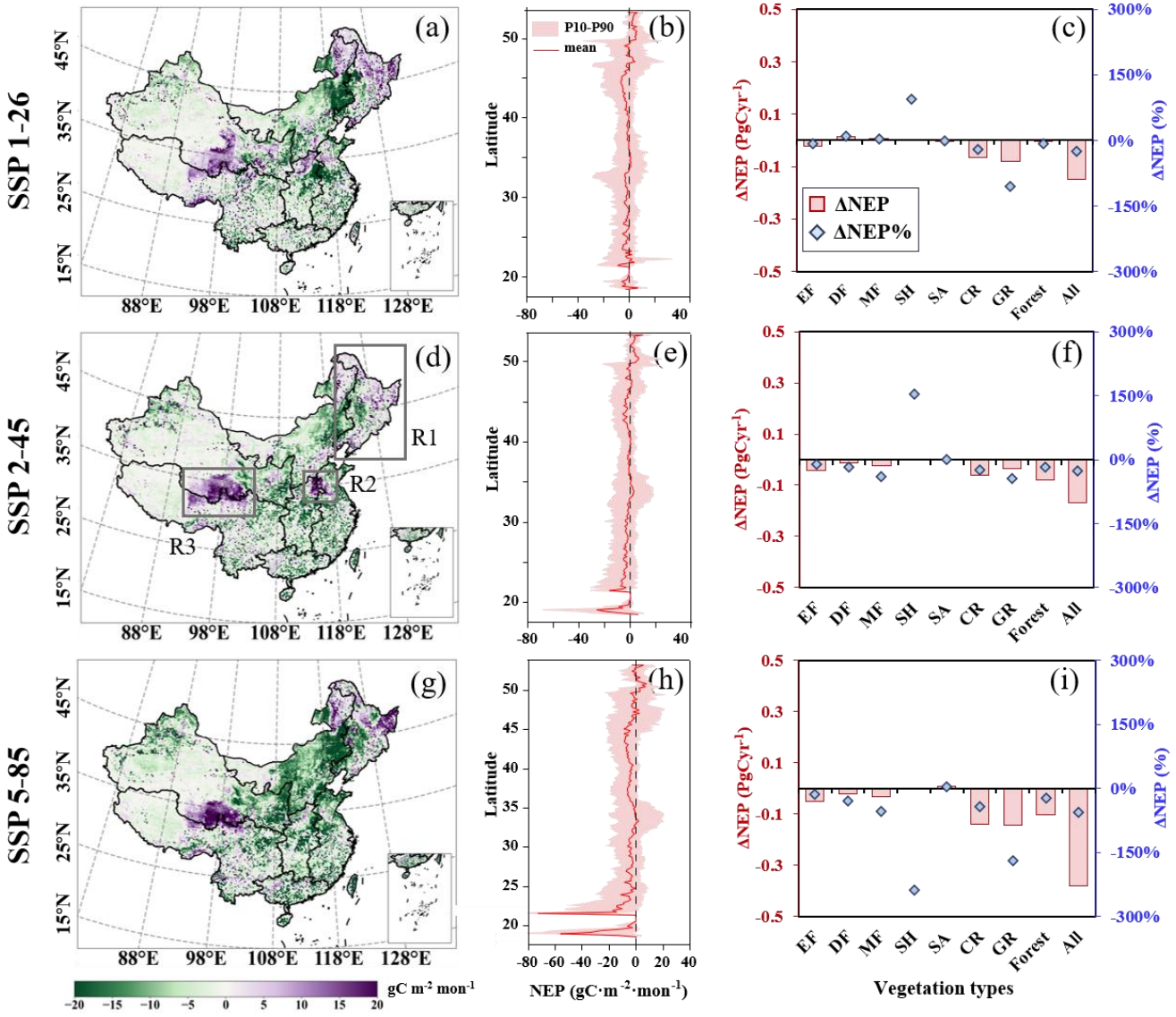


Figure 6. Changes in NEP in 2060 relative to the 2020 baseline under combined climate and land-cover changes across three SSP scenarios. (a, d, g) Spatial distribution of monthly ΔNEP (gC m^{-2} mon^{-1}); (b, e, h) Latitudinal zonal profiles of ΔNEP; (c, f, i) Absolute (red squares, Pg C yr^{-1}) and relative percentage (blue diamonds, %) changes in NEP for seven vegetation types. The top, middle and bottom rows represent SSP1-2.6, SSP2-4.5 and SSP5-8.5 scenarios, respectively. Abbreviations: EF – evergreen forest, DF – deciduous forest, MF – mixed forest, SH – shrubland, SA – savanna, CR – cropland, GR – grassland.

3.5 Modulation of warming-induced carbon sink weakening by vegetation dynamics

The projected weakening of the terrestrial carbon sink under warming is primarily driven by the direct temperature response of NEP, but this trend can be modulated by LULC transitions and in-situ vegetation dynamics (represented here via growing-

https://doi.org/10.5194/egusphere-2026-6317
Preprint. Discussion started: 11 November 2026
© Author(s) 2026. CC BY 4.0 License.

season EVI, GSEVI). Comparing the combined climate–LULC–GSEVI scenario against the climate-only forcing reveals that although long-term national trends remain dominated by rising temperature effects, LULC shifts and vegetation greening can partially buffer NEP decline in certain regions and periods. For example, by 2060 under SSP1-2.6, the overall NEP reduction reaches −24% (Fig. 5a, green line), compared with a −31% loss under climate-only forcing (Fig. 5a, grey line). Under SSP2-4.5, the combined NEP decline is −27%, less severe than the −39% loss simulated when only climate change is considered. Under high-emission SSP5-8.5, the projected total NEP reduction reaches −56%, still milder than the −63% decline from climate-only forcing.

To unpack these heterogeneous regional modulations, we selected three representative regions (R1 in Northeast China; R2 in North China cropland region; R3 in Southern Tibetan Plateau, marked in Fig.6d), which exhibit contrasting responses deviating from the pure temperature sensitivity test. In R1 (Fig. 7a-d), deciduous forests and croplands dominate the landscape. Under SSP2-4.5, GSEVI is projected to increase by 6–7% during the growing season (Fig.7c), accompanied by a 4–5% expansion of forest and cropland area. Climate warming alone reduces regional NEP by −3.8 gC m^{-2} mon^{-1} (a 13% loss). LULC transitions increase NEP by 1.1 gC m^{-2} mon^{-1} (4%), while dynamic GSEVI changes (including both land-conversion-induced vegetation replacement and within-type greening) further enhance NEP by 4.4 gC m^{-2} mon^{-1} (15%) (Fig.7b). Collectively, enhanced vegetation productivity fully offsets warming-induced NEP suppression, leading to a net NEP gain of 1.7 gC m^{-2} mon^{-1} (+6%) for R1 (Fig. 7d). This pattern aligns with widely documented vegetation greening across China over recent decades, driven by interactive effects of climate change, CO_2 fertilization and land management (Piao et al., 2013).

R2 is dominated by intensive croplands (Fig.7e). The 2020 baseline NEP is relatively low, representing a weak terrestrial carbon sink (Fig.7f). Climate warming substantially reduces regional NEP, pushing the ecosystem from a weak carbon sink toward a carbon source. Projected LULC transitions are minimal and contribute only minor NEP change (+0.1 gC m^{-2} mon^{-1}). In contrast, widespread strong greening (rising GSEVI, Fig. 7g) produces a large NEP gain of 28.1 gC m^{-2} mon^{-1}. The final net NEP increases by 13.1 gC m^{-2} mon^{-1}. We note this very large relative percentage increase (~400%) arises from the small baseline NEP magnitude and should not be interpreted as an enormous absolute carbon sink enhancement.

R3 located in the Southern Tibetan Plateau, dominated by grasslands (Fig. 7i). Unlike R1 and R2, climate warming increases regional NEP slightly (0.4 gC m^{-2} mon^{-1}, 3%). Together with LULC change and accompany greening (Fig. 7k) bring 1.6 gC m^{-2} mon^{-1} (11%) increase in NEP. This high-elevation region has cool background temperatures and sits on the ascending limb of the NEP–temperature response curve, where moderate warming relieves cold limitations on vegetation carbon uptake (Zhang et al., 2025b). It should be noted that this positive NEP anomalies to climate change represent a localized response to warming, though this result carries relatively higher uncertainty given sparse observational constraints for grassland ecosystems in this region.

Despite these substantial local buffering effects, they are insufficient to reverse the national-scale declining trend in NEP. Zonal-mean NEP remains negative across most latitude bands, with the strongest and most consistent sink loss

https://doi.org/10.5194/egusphere-2026-6317
Preprint. Discussion started: 11 November 2026
© Author(s) 2026. CC BY 4.0 License.

concentrated between 21–38°N, particularly under SSP5-8.5. Only the 48–53.3°N latitude band shows positive NEP anomalies across all three SSP scenarios, with the largest gain under SSP1-2.6. This high-latitude positive signal emerges from combined release of cold temperature constraints and improved vegetation growing conditions. Overall, although LULC shifts and vegetation dynamics can locally mitigate warming-induced carbon sink weakening, these modulating effects cannot override the dominant negative trend driven by rising air temperature across China.

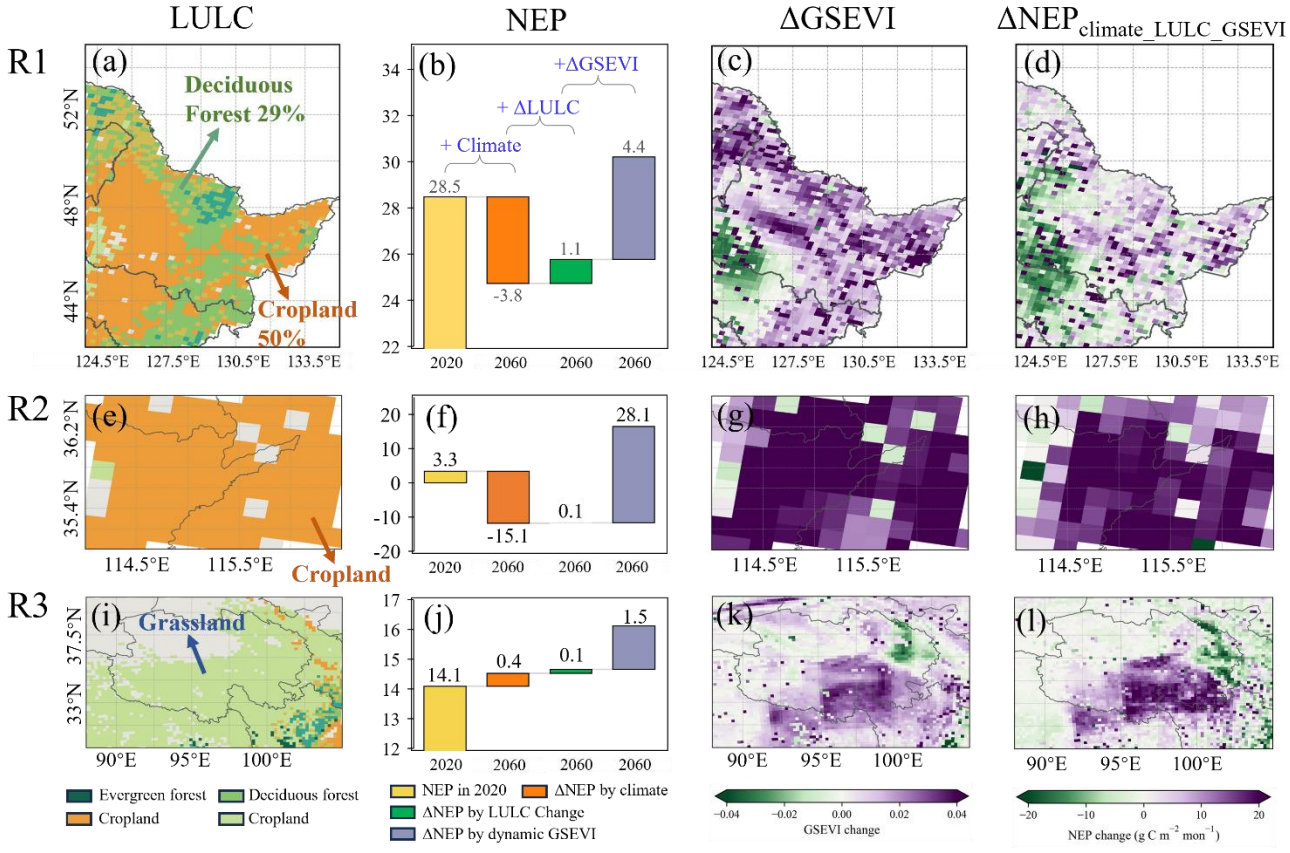


Figure 7. Regional drivers of NEP change from 2020 to 2060 under SSP2-45 for three representative areas. Rows correspond to R1 in Northeast China, R2 in North China and R3 in Southern Tibetan Plateau. Columns show (a,e,i) Dominate LULC classification; (b,f,j) quantitative attribution of regional NEP changes. Yellow bars denote baseline NEP in 2020; orange, green and blue bars represent NEP changes induced by climate warming, LULC transitions and dynamic GSEVI change, respectively. (c,g,k) Spatial pattern of GSEVI change (ΔGSEVI). Positive ΔGSEVI indicates enhanced vegetation greenness. (d,h,l) Spatial pattern of total NEP change ($\Delta NEP_{climate_LULC_GSEVI}$; unit: gC m^{-2} mon^{-1}) under combined climate, LULC and GSEVI changes.

https://doi.org/10.5194/egusphere-2026-6317
Preprint. Discussion started: 11 November 2026
© Author(s) 2026. CC BY 4.0 License.

4 Discussion

A weakened terrestrial carbon sink reduces the capacity of ecosystems to offset anthropogenic CO_2 emissions, complicating progress toward China's carbon peaking and carbon neutrality goals. To quantify the role of terrestrial carbon sinks in climate mitigation, we defined the carbon offset ratio (COR) as the annual ratio of NEP to anthropogenic carbon emissions. This metric provides a direct measure of the relative contribution of natural terrestrial sinks to offsetting fossil-fuel-related anthropogenic emissions.

As shown in Fig. 8, anthropogenic carbon emissions are projected to peak around 2030 before declining, while terrestrial NEP exhibits a steady weakening trend over the same period, leading to a shrinking COR by mid-century. This divergence between emission trajectories and sink dynamics underscores the growing reliance on direct emission reductions to meet climate targets, as natural sinks alone become increasingly insufficient to offset rising or even declining anthropogenic emissions.

Over the historical period (2005–2020), baseline simulations show that terrestrial ecosystems offset 10.9–18.3% of national anthropogenic emissions, with a gradual increasing trend. However, as warming intensifies, this offset capacity is projected to decline, even under divergent emission pathways. In the future baseline scenario, COR does not decline monotonically but exhibits distinct trends across SSP pathways. Under SSP1-26, COR rose from 12.3% in 2025 to 14.4% in 2030, driven by initial sink strength, before declining sharply to 7.5% by 2060. Under SSP2-45, COR decreased steadily from 15.4% to 8.0% between 2025 and 2060, with minor fluctuations. Under SSP5-85 scenario, COR remained low in the near-term and dropped precipitously after 2030, reaching only 2.2% by 2060. Before 2040, COR values were similar across baseline and clean-air pathways, indicating that near-term differences in emission trajectories had limited influence on this relative sink contribution. However, substantial divergence emerged after 2040 under early peak to net zero pathways.

Ambitious mitigation pathways significantly improved COR in the 2050s and 2060s across all SSPs, primarily by reducing anthropogenic emissions rather than enhancing sink capacity. For example, under SSP126 in 2060, COR increased from 7.5% under the baseline pathway to 100% under the two most ambitious mitigation pathways. Similar improvements were observed under SSP245, where COR also rose sharply under strong mitigation scenarios. In contrast, gains were more limited under SSP585, where high baseline emissions continued to outpace sink capacity even under mitigation.

Despite these relative improvements, terrestrial carbon sinks cannot substitute for direct anthropogenic emission reductions, as their absolute offset capacity weakens with ongoing warming. Overall, while terrestrial ecosystems have provided measurable carbon offsetting in the past, their future contribution is likely to become increasingly uncertain and limited under climate change.

https://doi.org/10.5194/egusphere-2026-6317
Preprint. Discussion started: 11 November 2026
© Author(s) 2026. CC BY 4.0 License.

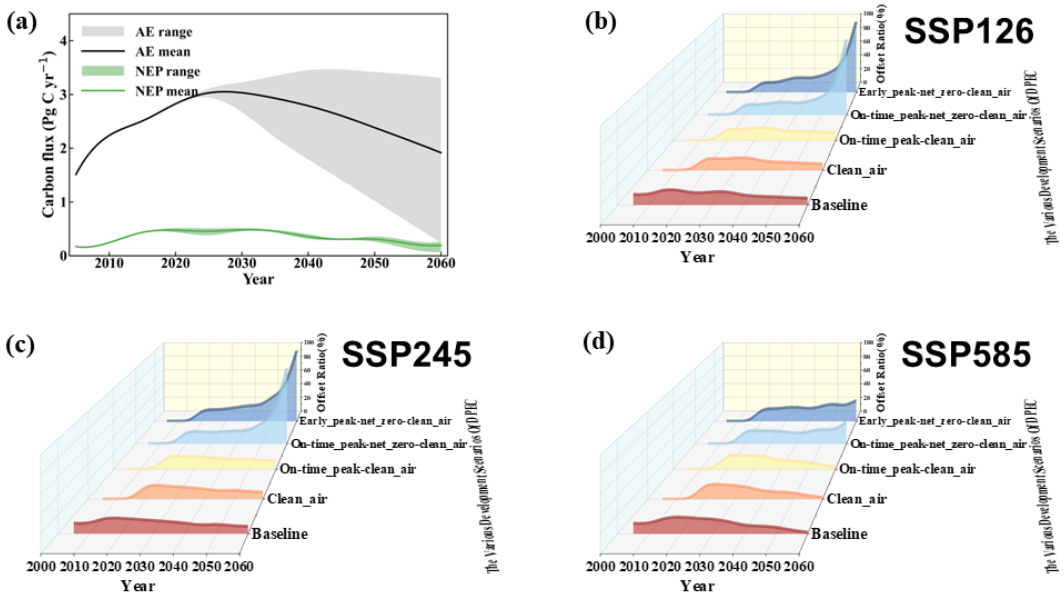


Figure 8. Changes in terrestrial carbon-offset ratio under diverse emission-mitigation scenarios. (a) Temporal changes of AE and NEP carbon fluxes. The AE mean and range denote the average and minimum-maximum range among six emission scenarios. The NEP mean and range denote the average and minimum-maximum range among three SSP pathways. (b-d) Carbon offset ratio under five mitigation pathways across three climate scenarios. Historical anthropogenic carbon emissions for 2000–2020 were obtained from MEIC, while historical COR analysis was conducted for 2005–2020 based on the available NEP simulations. Future anthropogenic carbon emissions for 2025–2060 were obtained from DPECv1.2.

This study quantified responses of terrestrial NEP to meteorological conditions and LULC change based on WRF-VPRM simulations and machine-learning approaches. Although the simplified parameterization of photosynthesis and ecosystem respiration facilitates model calibration against eddy-covariance observations, inherent deviations from real-world terrestrial biosphere processes still exist. Multiple fine-scale ecological factors not explicitly incorporated in this framework may regulate real-world NEP variations, including forest-age structure, cloud-radiation interactions and post-disturbance vegetation recovery (Leng et al., 2024). Such small-scale effects are implicitly averaged out at our regional grid scale. Unresolved microscale processes bring non-negligible uncertainties when extrapolating regional-scale findings down to finer local scales.

In addition, parts of the high-temperature flux-response relationships at site-scale rely on statistical extrapolation due to sparse in-situ observations (Fig. 2). Our XGBoost model was trained on gridded outputs from the calibrated WRF-VPRM simulation rather than direct in-situ flux measurements. Accordingly, machine-learning outputs inherit biases originating from the process-based model. Future EVI trajectories used in projections are derived from statistical extrapolation and cannot fully separate individual contributions from CO_2 fertilization, climate variability and land-management practices.

https://doi.org/10.5194/egusphere-2026-6317
Preprint. Discussion started: 11 November 2026
© Author(s) 2026. CC BY 4.0 License.

Besides, this study adopted fixed statistical thermal-response turning points derived from contemporary-condition simulations, whereas long-term warming may shift such response features through physiological acclimation and species compositional shifts (Fang et al., 2024). Moreover, insufficient long-term field observations constrain model validation under extreme climatic conditions. Drought, compound heat-drought stress and other extreme events can severely inhibit vegetation growth and carbon sequestration (Qi et al., 2025; Gu et al., 2025). Limited sample coverage of extreme cases may lead to biased NEP projections in climate-vulnerable regions, potentially causing overestimation or underestimation of future carbon-sink trends (He et al., 2023; Pastorello et al., 2020; Jiang et al., 2016).

5 Conclusions

This study integrated the WRF-VPRM model and XGBoost machine learning approach to explore nonlinear NEP-temperature relationships and assessed spatiotemporal variations in China's terrestrial carbon sink under changing climate and land cover conditions. Site observations confirm widespread nonlinear responses of NEP to temperature across diverse vegetation types, with distinct thermal thresholds separating rising and declining carbon sequestration capacity. Site-scale observations reveal vegetation-specific turning points in NEP–temperature relationships, yielding a broad range of NEP temperature thresholds spanning 15–25 °C. Aggregated to the national scale, NEP remains stable between 0 and 18 °C, peaks near 20 °C (18–22 °C), and declines beyond this optimum threshold, implying that sustained warming could weaken terrestrial carbon sequestration. A controlled sensitivity experiment with uniform 0.5 °C warming reduces national NEP by 0.17 PgC yr^{-1}, corresponding to a 31% loss of the terrestrial carbon sink. Future projections under three SSP scenarios show that carbon sink degradation intensifies with growing emission intensity. Near-term NEP changes remain small around 2030, ranging from −2% to +6%, whereas by 2060 national NEP is projected to decrease by 24%, 27%, and 56% under SSP126, SSP245, and SSP585, respectively. Across all three scenarios, grasslands exhibit the highest proportional vulnerability to warming, with NEP losses ranging from 44% to 171%, whereas forests show comparatively modest relative NEP declines (7–23%). While land-use and vegetation dynamics can partially offset these sink losses, such buffering effects remain localized and are overwhelmed by nationwide warming-driven carbon sink reduction. The declined carbon sink capacity caused an overall weakened carbon offset capacity by terrestrial ecosystem. Terrestrial ecosystems offset 10.9–18.3% of national anthropogenic emissions during 2005–2020, whereas future baseline COR declined to 7.5%, 8.0%, and 2.2% by 2060 under SSP126, SSP245, and SSP585, respectively. Overall, persistent warming poses substantial threats to the stability of China's terrestrial carbon sink. The findings deepen the understanding of temperature-driven carbon sink evolution and provide a reliable scientific basis for formulating targeted carbon management strategies and advancing dual-carbon goals.

https://doi.org/10.5194/egusphere-2026-6317
Preprint. Discussion started: 11 November 2026
© Author(s) 2026. CC BY 4.0 License.

Code and data availability

In-situ eddy covariance observations of ChinaFLUX network are available at https://chinaflux.org. The NCEP FNL reanalysis dataset is available at http://rda.ucar.edu/datasets/ds083.2. The MODIS land cover product MCD12Q1 and surface reflectance product MOD09A1 v6.1 are available at https://ladsweb.modaps.eosdis.nasa.gov. The CAMS-EGG4 data is available at https://ads.atmosphere.copernicus.eu. Historical anthropogenic carbon emissions of MEIC and future emissions of DPECv1.2 are available at http://meicmodel.org.cn. Future climate datasets are available from Zhang et al. (2025a). Future LULC trajectories are available from Hou et al. (2022). Modelling results of NEP (2020-2060) are available at https://zenodo.org/records/20424094. The source code of the WRF-VPRM model is archived in the UCAR data repository (https://www.bgc-jena.mpg.de/4758306/bsi_vprmpreproc). The code for data processing was written in python and is available upon request.

Author contributions

J.T. and **L.L.** conceived and designed this study. **B.X. and J.W.** collected and processed the in-situ measurements. **Y.W.** conducted the WRF-VPRM simulation. **B.X.** performed the XGBoost model and analyzed the data, with guidance from **J.T.** and **L.L.**

B.X. and J.T. wrote the manuscript. **H.D., L.H. and L.L.** reviewed and modified the manuscript.

Competing interests

The authors declare no competing financial or non-financial interests.

Acknowledgements

We acknowledge the support of the Shanghai Technical Service Center of Science and Engineering Computing, Shanghai University.

Financial support

This study was supported by the National Key Research and Development Program of China (No. 2023YFC3708601) and the Key Laboratory of Formation and Prevention of Urban Air Pollution Complex, Ministry of Ecology and Environment (No. 2025080164).

https://doi.org/10.5194/egusphere-2026-6317
Preprint. Discussion started: 11 November 2026
© Author(s) 2026. CC BY 4.0 License.

References

Ahmadov, R., Gerbig, C., Kretschmer, R., Koerner, S., Neininger, B., Dolman, A. J., and Sarrat, C.: Mesoscale covariance of transport and CO2 fluxes: Evidence from observations and simulations using the WRF-VPRM coupled atmosphere-biosphere model, Journal of Geophysical Research: Atmospheres, 112, D22107, 10.1029/2007jd008552, 2007.

Amthor, J. S., Chen, J. M., Clein, J. S., Frolking, S. E., Goulden, M. L., Grant, R. F., Kimball, J. S., King, A. W., McGuire, A. D., Nikolov, N. T., Potter, C. S., Wang, S., and Wofsy, S. C.: Boreal forest CO2 exchange and evapotranspiration predicted by nine ecosystem process models: Intermodel comparisons and relationships to field measurements, Journal of Geophysical Research: Atmospheres, 106, 33623-33648, 10.1029/2000jd900850, 2001.

Bai, J., Chang, I. S., Zhang, C., and Wu, J.: Allocation of CO2 emission target in China under the "1 + N" policy: Considering natural carbon sinks and wind-solar-hydropower endowments, Environmental Impact Assessment Review, 106, 107472, 10.1016/j.eiar.2024.107472, 2024.

Berthelot, M., Friedlingstein, P., Ciais, P., Dufresne, J. L., and Monfray, P.: How uncertainties in future climate change predictions translate into future terrestrial carbon fluxes, Global Change Biology, 11, 959-970, 10.1111/j.1365-2486.2005.00957.x, 2005.

Chen, T. and Guestrin, C.: XGBoost: A Scalable Tree Boosting System, Proceedings of the 22nd ACM SIGKDD International Conference on Knowledge Discovery and Data Mining, 10.1145/2939672.2939785, 2016.

Corlett, R. T.: Impacts of warming on tropical lowland rainforests, Trends Ecol Evol, 26, 606-613, 10.1016/j.tree.2011.06.015, 2011.

Cramer, W., Bondeau, A., Woodward, F. I., Prentice, I. C., Betts, R. A., Brovkin, V., Cox, P. M., Fisher, V., Foley, J. A., Friend, A. D., Kucharik, C., Lomas, M. R., Ramankutty, N., Sitch, S., Smith, B., White, A., and Young-Molling, C.: Global response of terrestrial ecosystem structure and function to CO2 and climate change: results from six dynamic global vegetation models, Global Change Biology, 7, 357–373, 10.1046/j.1365-2486.2001.00383.x, 2001.

Doughty, C. E. and Goulden, M. L.: Are tropical forests near a high temperature threshold?, Journal of Geophysical Research: Biogeosciences, 113, G00B07, 10.1029/2007JG000632, 2008.

Dwivedi, R., Dave, D., Naik, H., Singhal, S., Omer, R., Patel, P., Qian, B., Wen, Z., Shah, T., Morgan, G., and Ranjan, R.: Explainable AI (XAI): Core Ideas, Techniques, and Solutions, ACM Computing Surveys, 55, 1-33, 10.1145/3561048, 2023.

Fang, Z., Zhang, W., Wang, L., Schurgers, G., Ciais, P., Peñuelas, J., Brandt, M., Yang, H., Huang, K., Shen, Q., and Fensholt, R.: Global increase in the optimal temperature for the productivity of terrestrial ecosystems, Communications Earth & Environment, 5, 466, 10.1038/s43247-024-01636-9, 2024.

Fernández-Martínez, M., Sardans, J., Chevallier, F., Ciais, P., Obersteiner, M., Vicca, S., Canadell, J. G., Bastos, A., Friedlingstein, P., Sitch, S., Piao, S. L., Janssens, I. A., and Peñuelas, J.: Global trends in carbon sinks and their relationships with CO2 and temperature, Nature Climate Change, 9, 73-79, 10.1038/s41558-018-0367-7, 2019.

Friedlingstein, P., Le Quere, C., O'Sullivan, M., Hauck, J., Landschutzer, P., Luijkx, I. T., Li, H., van der Woude, A., Schwingshackl, C., Pongratz, J., Regnier, P., Andrew, R. M., Bakker, D. C. E., Canadell, J. G., Ciais, P., Gasser, T., Jones, M. W., Lan, X., Morgan, E., Olsen, A., Peters, G. P., Peters, W., Sitch, S., and Tian, H.: Emerging climate impact on carbon sinks in a consolidated carbon budget, Nature, 649, 98-103, 10.1038/s41586-025-09802-5, 2026.

Friedlingstein, P., Cox, P., Betts, R., Bopp, L., von Bloh, W., Brovkin, V., Cadule, P., Doney, S., Eby, M., Fung, I., Bala, G., John, J., Jones, C., Joos, F., Kato, T., Kawamiya, M., Knorr, W., Lindsay, K., Matthews, H. D., Raddatz, T., Rayner, P., Reick, C., Roeckner, E., Schnitzler, K.-G., Schnur, R., Strassmann, K., Weaver, A. J., Yoshikawa, C., and Zeng, N.: Climate–Carbon Cycle Feedback Analysis: Results from the C4MIP Model Intercomparison, Journal of Climate, 19, 3337–3353, 10.1175/JCLI3800.1, 2006.

Friedlingstein, P., O'Sullivan, M., Jones, M. W., Andrew, R. M., Gregor, L., Hauck, J., Le Quéré, C., Luijkx, I. T., Olsen, A., Peters, G. P., Peters, W., Pongratz, J., Schwingshackl, C., Sitch, S., Canadell, J. G., Ciais, P., Jackson, R. B., Alin, S. R., Alkama, R., Arneth, A., Arora, V. K., Bates, N. R., Becker, M., Bellouin, N., Bittig, H. C., Bopp, L., Chevallier, F., Chini, L. P., Cronin, M., Evans, W., Falk, S., Feely, R. A., Gasser, T., Gehlen, M., Gkritzalis, T., Gloege, L., Grassi, G., Gruber, N., Gürses, Ö., Harris, I., Hefner, M., Houghton, R. A., Hurtt, G. C., Iida, Y., Ilyina, T., Jain, A. K., Jersild, A., Kadono, K., Kato, E., Kennedy, D., Klein Goldewijk, K., Knauer, J., Korsbakken, J. I., Landschützer, P., Lefèvre, N., Lindsay, K., Liu, J., Liu, Z., Marland, G., Mayot, N., McGrath, M. J., Metzl, N., Monacci, N. M., Munro, D. R.,

https://doi.org/10.5194/egusphere-2026-6317
Preprint. Discussion started: 11 November 2026
© Author(s) 2026. CC BY 4.0 License.

Nakaoka, S.-I., Niwa, Y., O'Brien, K., Ono, T., Palmer, P. I., Pan, N., Pierrot, D., Pocock, K., Poulter, B., Resplandy, L., Robertson, E., Rödenbeck, C., Rodriguez, C., Rosan, T. M., Schwinger, J., Séférian, R., Shutler, J. D., Skjelvan, I., Steinhoff, T., Sun, Q., Sutton, A. J., Sweeney, C., Takao, S., Tanhua, T., Tans, P. P., Tian, X., Tian, H., Tilbrook, B., Tsujino, H., Tubiello, F., van der Werf, G. R., Walker, A. P., Wanninkhof, R., Whitehead, C., Willstrand Wranne, A., Wright, R., Yuan, W., Yue, C., Yue, X., Zaehle, S., Zeng, J., and Zheng, B.: Global Carbon Budget 2022, Earth System Science Data, 14, 4811-4900, 10.5194/essd-14-4811-2022, 2022.

Fu, C., Wang, G., Yang, Y., Wu, H., Wu, H., Zhang, H., and Xia, Y.: Temperature Thresholds for Carbon Flux Variation and Warming-Induced Changes, Journal of Geophysical Research: Atmospheres, 128, e2023JD039747, 10.1029/2023jd039747, 2023.

Fu, J., Li, P., Lin, Y., Du, H., Liu, H., Zhu, W., and Ren, H.: Fight for carbon neutrality with state-of-the-art negative carbon emission technologies, Eco Environ Health, 1, 259-279, 10.1016/j.eehl.2022.11.005, 2022.

García-Martínez, J. and Hartshorn, R. M.: Feeding the Planet: The Main Contribution and Challenge of Chemistry, ACS Agricultural Science & Technology, 3, 457-459, 10.1021/acsagscitech.3c00108, 2023.

Gidden, M. J., Riahi, K., Smith, S. J., Fujimori, S., Luderer, G., Kriegler, E., van Vuuren, D. P., van den Berg, M., Feng, L., Klein, D., Calvin, K., Doelman, J. C., Frank, S., Fricko, O., Harmsen, M., Hasegawa, T., Havlik, P., Hilaire, J., Hoesly, R., Horing, J., Popp, A., Stehfest, E., and Takahashi, K.: Global emissions pathways under different socioeconomic scenarios for use in CMIP6: a dataset of harmonized emissions trajectories through the end of the century, Geoscientific Model Development, 12, 1443-1475, 10.5194/gmd-12-1443-2019, 2019.

Gu, L., Schumacher, D. L., Fischer, E. M., Slater, L. J., Yin, J., Sippel, S., Chen, J., Liu, P., and Knutti, R.: Flash drought impacts on global ecosystems amplified by extreme heat, Nature Geoscience, 18, 709-715, 10.1038/s41561-025-01719-y, 2025.

He, W., Jiang, F., Ju, W., Chevallier, F., Baker, D. F., Wang, J., Wu, M., Johnson, M. S., Philip, S., Wang, H., Bertolacci, M., Liu, Z., Zeng, N., and Chen, J. M.: Improved Constraints on the Recent Terrestrial Carbon Sink Over China by Assimilating OCO-2 XCO2 Retrievals, Journal of Geophysical Research: Atmospheres, 128, e2022JD037773, 10.1029/2022jd037773, 2023.

He, W., Jiang, F., Wu, M., Ju, W., Scholze, M., Chen, J. M., Byrne, B., Liu, J., Wang, H., Wang, J., Wang, S., Zhou, Y., Zhang, C., Nguyen, N. T., Shen, Y., and Chen, Z.: China's Terrestrial Carbon Sink Over 2010–2015 Constrained by Satellite Observations of Atmospheric CO2 and Land Surface Variables, Journal of Geophysical Research: Biogeosciences, 127, e2021JG006644, 10.1029/2021jg006644, 2022.

Hou, H., Zhou, B. B., Pei, F., Hu, G., Su, Z., Zeng, Y., Zhang, H., Gao, Y., Luo, M., and Li, X.: Future Land Use/Land Cover Change Has Nontrivial and Potentially Dominant Impact on Global Gross Primary Productivity, Earth's Future, 10, e2021EF002628, 10.1029/2021ef002628, 2022.

Huang, M., Piao, S., Ciais, P., Penuelas, J., Wang, X., Keenan, T. F., Peng, S., Berry, J. A., Wang, K., Mao, J., Alkama, R., Cescatti, A., Cuntz, M., De Deurwaerder, H., Gao, M., He, Y., Liu, Y., Luo, Y., Myneni, R. B., Niu, S., Shi, X., Yuan, W., Verbeeck, H., Wang, T., Wu, J., and Janssens, I. A.: Air temperature optima of vegetation productivity across global biomes, Nat Ecol Evol, 3, 772-779, 10.1038/s41559-019-0838-x, 2019.

Jiang, F., Chen, J. M., Zhou, L., Ju, W., Zhang, H., Machida, T., Ciais, P., Peters, W., Wang, H., Chen, B., Liu, L., Zhang, C., Matsueda, H., and Sawa, Y.: A comprehensive estimate of recent carbon sinks in China using both top-down and bottom-up approaches, Sci Rep, 6, 22130, 10.1038/srep22130, 2016.

Kou, X., Peng, Z., Zhang, M., Hu, F., Han, X., Li, Z., and Lei, L.: The carbon sink in China as seen from GOSAT with a regional inversion system based on the Community Multi-scale Air Quality (CMAQ) and ensemble Kalman smoother (EnKS), Atmospheric Chemistry and Physics, 23, 6719-6741, 10.5194/acp-23-6719-2023, 2023.

Krause, A., Papastefanou, P., Gregor, K., Layritz, L. S., Zang, C. S., Buras, A., Li, X., Xiao, J., and Rammig, A.: Quantifying the impacts of land cover change on gross primary productivity globally, Sci Rep, 12, 18398, 10.1038/s41598-022-23120-0, 2022.

Leng, Y., Li, W., Ciais, P., Sun, M., Zhu, L., Yue, C., Chang, J., Yao, Y., Zhang, Y., Zhou, J., Li, Z., Wang, X., Xi, Y., and Peng, S.: Forest aging limits future carbon sink in China, One Earth, 7, 822-834, 10.1016/j.oneear.2024.04.011, 2024.

Li, X., Hu, X. M., Cai, C., Jia, Q., Zhang, Y., Liu, J., Xue, M., Xu, J., Wen, R., and Crowell, S. M. R.: Terrestrial CO2 Fluxes, Concentrations, Sources and Budget in Northeast China: Observational and Modeling Studies, Journal of Geophysical Research: Atmospheres, 125, e2019JD031686, 10.1029/2019jd031686, 2020.

https://doi.org/10.5194/egusphere-2026-6317
Preprint. Discussion started: 11 November 2026
© Author(s) 2026. CC BY 4.0 License.

Lundberg, S. M. and Lee, S.-I.: A Unified Approach to Interpreting Model Predictions, In Proceedings of the 31st International Conference on Neural Information Processing Systems (NeurIPS 2017), 4765-4774, 10.48550/arXiv.1705.07874, 2017.

Mahadevan, P., Wofsy, S. C., Matross, D. M., Xiao, X., Dunn, A. L., Lin, J. C., Gerbig, C., Munger, J. W., Chow, V. Y., and Gottlieb, E. W.: A satellite-based biosphere parameterization for net ecosystem CO2 exchange: Vegetation Photosynthesis and Respiration Model (VPRM), Global Biogeochemical Cycles, 22, GB2005, 10.1029/2006gb002735, 2008.

Merabet, K., Di Nunno, F., Granata, F., Kim, S., Adnan, R. M., Heddam, S., Kisi, O., and Zounemat-Kermani, M.: Predicting water quality variables using gradient boosting machine: global versus local explainability using SHapley Additive Explanations (SHAP), Earth Science Informatics, 18, 298, 10.1007/s12145-025-01796-y, 2025.

Niu, S., Luo, Y., Fei, S., Yuan, W., Schimel, D., Law, B. E., Ammann, C., Altaf Arain, M., Arneth, A., Aubinet, M., Barr, A., Beringer, J., Bernhofer, C., Andrew Black, T., Buchmann, N., Cescatti, A., Chen, J., Davis, K. J., Dellwik, E., Desai, A. R., Etzold, S., Francois, L., Gianelle, D., Gielen, B., Goldstein, A., Groenendijk, M., Gu, L., Hanan, N., Helfter, C., Hirano, T., Hollinger, D. Y., Jones, M. B., Kiely, G., Kolb, T. E., Kutsch, W. L., Lafleur, P., Lawrence, D. M., Li, L., Lindroth, A., Litvak, M., Loustau, D., Lund, M., Marek, M., Martin, T. A., Matteucci, G., Migliavacca, M., Montagnani, L., Moors, E., William Munger, J., Noormets, A., Oechel, W., Olejnik, J., U, K. T. P., Pilegaard, K., Rambal, S., Raschi, A., Scott, R. L., Seufert, G., Spano, D., Stoy, P., Sutton, M. A., Varlagin, A., Vesala, T., Weng, E., Wohlfahrt, G., Yang, B., Zhang, Z., and Zhou, X.: Thermal optimality of net ecosystem exchange of carbon dioxide and underlying mechanisms, New Phytologist, 194, 775-783, 10.1111/j.1469-8137.2012.04095.x, 2012.

Park, C., Gerbig, C., Newman, S., Ahmadov, R., Feng, S., Gurney, K. R., Carmichael, G. R., Park, S.-Y., Lee, H.-W., Goulden, M., Stutz, J., Peischl, J., and Ryerson, T.: CO2 Transport, Variability, and Budget over the Southern California Air Basin Using the High-Resolution WRF-VPRM Model during the CalNex 2010 Campaign, Journal of Applied Meteorology and Climatology, 57, 1337-1352, 10.1175/jamc-d-17-0358.1, 2018.

Pastorello, G., Trotta, C., Canfora, E., Chu, H., Christianson, D., Cheah, Y. W., Poindexter, C., Chen, J., Elbashandy, A., Humphrey, M., Isaac, P., Polidori, D., Reichstein, M., Ribeca, A., van Ingen, C., Vuichard, N., Zhang, L., Amiro, B., Ammann, C., Arain, M. A., Ardo, J., Arkebauer, T., Arndt, S. K., Arriga, N., Aubinet, M., Aurela, M., Baldocchi, D., Barr, A., Beamesderfer, E., Marchesini, L. B., Bergeron, O., Beringer, J., Bernhofer, C., Berveiller, D., Billesbach, D., Black, T. A., Blanken, P. D., Bohrer, G., Boike, J., Bolstad, P. V., Bonal, D., Bonnefond, J. M., Bowling, D. R., Bracho, R., Brodeur, J., Brummer, C., Buchmann, N., Burban, B., Burns, S. P., Buysse, P., Cale, P., Cavagna, M., Cellier, P., Chen, S., Chini, I., Christensen, T. R., Cleverly, J., Collalti, A., Consalvo, C., Cook, B. D., Cook, D., Coursolle, C., Cremonese, E., Curtis, P. S., D'Andrea, E., da Rocha, H., Dai, X., Davis, K. J., Cinti, B., Grandcourt, A., Ligne, A., De Oliveira, R. C., Delpierre, N., Desai, A. R., Di Bella, C. M., Tommasi, P. D., Dolman, H., Domingo, F., Dong, G., Dore, S., Duce, P., Dufrene, E., Dunn, A., Dusek, J., Eamus, D., Eichelmann, U., ElKhidir, H. A. M., Eugster, W., Ewenz, C. M., Ewers, B., Famulari, D., Fares, S., Feigenwinter, I., Feitz, A., Fensholt, R., Filippa, G., Fischer, M., Frank, J., Galvagno, M., Gharun, M., Gianelle, D., Gielen, B., Gioli, B., Gitelson, A., Goded, I., Goeckede, M., Goldstein, A. H., Gough, C. M., Goulden, M. L., Graf, A., Griebel, A., Gruening, C., Grunwald, T., Hammerle, A., Han, S., Han, X., Hansen, B. U., Hanson, C., Hatakka, J., He, Y., Hehn, M., Heinesch, B., Hinko-Najera, N., Hortnagl, L., Hutley, L., Ibrom, A., Ikawa, H., Jackowicz-Korczynski, M., Janous, D., Jans, W., Jassal, R., Jiang, S., Kato, T., Khomik, M., Klatt, J., Knohl, A., Knox, S., Kobayashi, H., Koerber, G., Kolle, O., Kosugi, Y., Kotani, A., Kowalski, A., Kruijt, B., Kurbatova, J., Kutsch, W. L., Kwon, H., Launiainen, S., Laurila, T., Law, B., Leuning, R., Li, Y., Liddell, M., Limousin, J. M., Lion, M., Liska, A. J., Lohila, A., Lopez-Ballesteros, A., Lopez-Blanco, E., Loubet, B., Loustau, D., Lucas-Moffat, A., Luers, J., Ma, S., Macfarlane, C., Magliulo, V., Maier, R., Mammarella, I., Manca, G., Marcolla, B., Margolis, H. A., Marras, S., Massman, W., Mastepanov, M., Matamala, R., Matthes, J. H., Mazzenga, F., McCaughey, H., McHugh, I., McMillan, A. M. S., Merbold, L., Meyer, W., Meyers, T., Miller, S. D., Minerbi, S., Moderow, U., Monson, R. K., Montagnani, L., Moore, C. E., Moors, E., Moreaux, V., Moureaux, C., Munger, J. W., Nakai, T., Neirynck, J., Nesic, Z., Nicolini, G., Noormets, A., Northwood, M., Nosetto, M., Nouvellon, Y., Novick, K., Oechel, W., Olesen, J. E., Ourcival, J. M., Papuga, S. A., Parmentier, F. J., Paul-Limoges, E., Pavelka, M., Peichl, M., Pendall, E., Phillips, R. P., Pilegaard, K., Pirk, N., Posse, G., Powell, T., Prasse, H., Prober, S. M., Rambal, S., Rannik, U., Raz-Yaseef, N., Rebmann, C., Reed, D., Dios, V. R., Restrepo-Coupe, N., Reverter, B. R., Roland, M., Sabbatini, S., Sachs, T., Saleska, S. R., Sanchez-Canete, E. P., Sanchez-Mejia, Z. M., Schmid, H. P., Schmidt, M., Schneider, K., Schrader,

https://doi.org/10.5194/egusphere-2026-6317
Preprint. Discussion started: 11 November 2026
© Author(s) 2026. CC BY 4.0 License.

F., Schroder, I., Scott, R. L., Sedlak, P., Serrano-Ortiz, P., Shao, C., Shi, P., Shironya, I., Siebicke, L., Sigut, L., Silberstein, R., Sirca, C., Spano, D., Steinbrecher, R., Stevens, R. M., Sturtevant, C., Suyker, A., Tagesson, T., Takanashi, S., Tang, Y., Tapper, N., Thom, J., Tomassucci, M., Tuovinen, J. P., Urbanski, S., Valentini, R., van der Molen, M., van Gorsel, E., van Huissteden, K., Varlagin, A., Verfaillie, J., Vesala, T., Vincke, C., Vitale, D., Vygodskaya, N., Walker, J. P., Walter-Shea, E., Wang, H., Weber, R., Westermann, S., Wille, C., Wofsy, S., Wohlfahrt, G., Wolf, S., Woodgate, W., Li, Y., Zampedri, R., Zhang, J., Zhou, G., Zona, D., Agarwal, D., Biraud, S., Torn, M., and Papale, D.: The FLUXNET2015 dataset and the ONEFlux processing pipeline for eddy covariance data, Sci Data, 7, 225, 10.1038/s41597-020-0534-3, 2020.

Piao, S., He, Y., Wang, X., and Chen, F.: Estimation of China's terrestrial ecosystem carbon sink: Methods, progress and prospects, Science China Earth Sciences, 65, 641-651, 10.1007/s11430-021-9892-6, 2022.

Piao, S., Zhang, X., Chen, A., Liu, Q., Lian, X., Wang, X., Peng, S., and Wu, X.: The impacts of climate extremes on the terrestrial carbon cycle: A review, Science China Earth Sciences, 62, 1551-1563, 10.1007/s11430-018-9363-5, 2019.

Piao, S., Sitch, S., Ciais, P., Friedlingstein, P., Peylin, P., Wang, X., Ahlstrom, A., Anav, A., Canadell, J. G., Cong, N., Huntingford, C., Jung, M., Levis, S., Levy, P. E., Li, J., Lin, X., Lomas, M. R., Lu, M., Luo, Y., Ma, Y., Myneni, R. B., Poulter, B., Sun, Z., Wang, T., Viovy, N., Zaehle, S., and Zeng, N.: Evaluation of terrestrial carbon cycle models for their response to climate variability and to CO2 trends, Glob Chang Biol, 19, 2117-2132, 10.1111/gcb.12187, 2013.

Qi, G., Song, J., Chen, S., Gong, Y., Bai, H., She, D., Xia, J., and Fu, Y. H.: Increasing impacts of compound extreme droughts on vegetation productivity in China, Journal of Hydrology, 660, 133447, 10.1016/j.jhydrol.2025.133447, 2025.

Ruehr, S., Keenan, T. F., Williams, C., Zhou, Y., Lu, X., Bastos, A., Canadell, J. G., Prentice, I. C., Sitch, S., and Terrer, C.: Evidence and attribution of the enhanced land carbon sink, Nature Reviews Earth & Environment, 4, 518-534, 10.1038/s43017-023-00456-3, 2023.

Shen, N., Tan, J., Wang, W., Xue, W., Wang, Y., Huang, L., Yan, G., Song, Y., and Li, L.: Long-term changes of methane emissions from rice cultivation during 2000 - 2060 in China: Trends, driving factors, predictions and policy implications, Environ Int, 191, 108958, 10.1016/j.envint.2024.108958, 2024.

Sitch, S., Friedlingstein, P., Gruber, N., Jones, S. D., Murray-Tortarolo, G., Ahlström, A., Doney, S. C., Graven, H., Heinze, C., Huntingford, C., Levis, S., Levy, P. E., Lomas, M., Poulter, B., Viovy, N., Zaehle, S., Zeng, N., Arneth, A., Bonan, G., Bopp, L., Canadell, J. G., Chevallier, F., Ciais, P., Ellis, R., Gloor, M., Peylin, P., Piao, S. L., Le Quéré, C., Smith, B., Zhu, Z., and Myneni, R.: Recent trends and drivers of regional sources and sinks of carbon dioxide, Biogeosciences, 12, 653-679, 10.5194/bg-12-653-2015, 2015.

Tang, Y., Jia, C., Wang, L., Wen, X., and Wang, H.: Solar energy dominates and soil water modulates net ecosystem productivity and evapotranspiration across multiple timescales in a subtropical coniferous plantation, Agricultural and Forest Meteorology, 300, 108310, 10.1016/j.agrformet.2020.108310, 2021.

Toïgo, M., Nicolas, M., Jonard, M., Croisé, L., Nageleisen, L.-M., and Jactel, H.: Temporal trends in tree defoliation and response to multiple biotic and abiotic stresses, Forest Ecology and Management, 477, 118476, 10.1016/j.foreco.2020.118476, 2020.

Wang, L., Yu, M., Ye, S., and Yan, J.: Seasonal patterns of carbon and water flux responses to precipitation and solar radiation variability in a subtropical evergreen forest, South China, Agricultural and Forest Meteorology, 342, 109760, 10.1016/j.agrformet.2023.109760, 2023a.

Wang, M., Zhang, S., Guo, X., Xiao, L., Yang, Y., Luo, Y., Mishra, U., and Luo, Z.: Responses of soil organic carbon to climate extremes under warming across global biomes, Nature Climate Change, 14, 98-105, 10.1038/s41558-023-01874-3, 2023b.

Xia, X., Ren, P., Wang, X., Liu, D., Chen, X., Dan, L., He, B., He, H., Ju, W., Liang, M., Lu, X., Peng, J., Qin, Z., Xia, J., Zheng, B., Wei, J., Yue, X., Yu, G., Piao, S., and Yuan, W.: The carbon budget of China: 1980-2021, Sci Bull (Beijing), 69, 114-124, 10.1016/j.scib.2023.11.016, 2024.

Xiao, X., Hollinger, D., Aber, J., Goltz, M., Davidson, E. A., Zhang, Q., and Moore, B.: Satellite-based modeling of gross primary production in an evergreen needleleaf forest, Remote Sensing of Environment, 89, 519-534, 10.1016/j.rse.2003.11.008, 2004.

Xu, X., Xu, J., Li, B., Li, J., and Nie, M.: Ecosystem Carbon Fluxes Exhibit Thermal Response Thresholds at Which Carbon–Climate Feedback Changes, Global Ecology and Biogeography, 34, e70030, 10.1111/geb.70030, 2025.

https://doi.org/10.5194/egusphere-2026-6317
Preprint. Discussion started: 11 November 2026
© Author(s) 2026. CC BY 4.0 License.

Yu, G.-R., Wen, X.-F., Sun, X.-M., Tanner, B. D., Lee, X., and Chen, J.-Y.: Overview of ChinaFLUX and evaluation of its eddy covariance measurement, Agricultural and Forest Meteorology, 137, 125-137, https://doi.org/10.1016/j.agrformet.2006.02.011, 2006.

YU, G.-R., ZHANG, L.-M., SUN, X.-M., FU, Y.-L., WEN, X.-F., WANG, Q.-F., LI, S.-G., REN, C.-Y., SONG, X., LIU, Y.-F., HAN, S.-J., and YAN, J.-H.: Environmental controls over carbon exchange of three forest ecosystems in eastern China, Global Change Biology, 14, 2555-2571, 10.1111/j.1365-2486.2008.01663.x, 2008.

Yu, G., Chen, Z., Piao, S., Peng, C., Ciais, P., Wang, Q., Li, X., and Zhu, X.: High carbon dioxide uptake by subtropical forest ecosystems in the East Asian monsoon region, Proceedings of the National Academy of Sciences of the United States of America, 111, 4910-4915, 10.1073/pnas.1317065111, 2014.

Yuan, M., Zhu, Q., Zhang, J., Liu, J., Chen, H., Peng, C., Li, P., Li, M., Wang, M., and Zhao, P.: Global response of terrestrial gross primary productivity to climate extremes, Sci Total Environ, 750, 142337, 10.1016/j.scitotenv.2020.142337, 2021.

Yuan, X., Chen, X., Ochege, F. U., Hamdi, R., Tabari, H., Li, B., He, B., Zhang, C., De Maeyer, P., and Luo, G.: Weakening of global terrestrial carbon sequestration capacity under increasing intensity of warm extremes, Nature Ecology & Evolution, 9, 124-133, 10.1038/s41559-024-02576-5, 2025.

Yue, X., Liao, H., Wang, H., Zhang, T., Unger, N., Sitch, S., Feng, Z., and Yang, J.: Pathway dependence of ecosystem responses in China to 1.5 °C global warming, Atmospheric Chemistry and Physics, 20, 2353-2366, 10.5194/acp-20-2353-2020, 2020.

Yue, X., Zhou, H., Cao, Y., Liao, H., Lu, X., Yu, Z., Yuan, W., Liu, Z., Lei, Y., Sitch, S., Knauer, J., and Wang, H.: Large potential of strengthening the land carbon sink in China through anthropogenic interventions, Sci Bull (Beijing), 69, 2622-2631, 10.1016/j.scib.2024.05.037, 2024.

Yvon-Durocher, G., Jones, J. I., Trimmer, M., Woodward, G., and Montoya, J. M.: Warming alters the metabolic balance of ecosystems, Philosophical Transactions of the Royal Society B: Biological Sciences, 365, 2117-2126, 10.1098/rstb.2010.0038, 2010.

Yvon-Durocher, G., Caffrey, J. M., Cescatti, A., Dossena, M., del Giorgio, P., Gasol, J. M., Montoya, J. M., Pumpanen, J., Staehr, P. A., Trimmer, M., Woodward, G., and Allen, A. P.: Reconciling the temperature dependence of respiration across timescales and ecosystem types, Nature, 487, 472-476, 10.1038/nature11205, 2012.

Zhang, F., Li, X., Wang, X., Tan, M., and Xin, L.: CMIP6-driven 10 km super-resolution daily climate projections with PET estimates in China, Sci Data, 12, 720, 10.1038/s41597-025-05071-z, 2025a.

Zhang, X., Zhang, S., Zhou, J., and Fan, J.: Environmental thresholds triggering changes in above and belowground biomass carbon in China, Global Ecology and Conservation, 61, e03676, 10.1016/j.gecco.2025.e03676, 2025b.

Zhang, Z., Zhang, R., Cescatti, A., Wohlfahrt, G., Buchmann, N., Zhu, J., Chen, G., Moyano, F., Pumpanen, J., Hirano, T., Takagi, K., and Merbold, L.: Effect of climate warming on the annual terrestrial net ecosystem CO(2) exchange globally in the boreal and temperate regions, Sci Rep, 7, 3108, 10.1038/s41598-017-03386-5, 2017.

Zhong, J., Zhang, X., Guo, L., Wang, D., Miao, C., and Zhang, X.: Ongoing CO(2) monitoring verify CO(2) emissions and sinks in China during 2018-2021, Sci Bull (Beijing), 68, 2467-2476, 10.1016/j.scib.2023.08.039, 2023.